

# Large deformation electrohydrodynamics of an elastic capsule in DC electric field

Sudip Das and Rochish M. Thaokar

Department of Chemical Engineering, Indian Institute of Technology Bombay, Mumbai, 400076, India

## Abstract

The dynamics of a spherical elastic capsule, containing a Newtonian fluid bounded by an elastic membrane and immersed in another Newtonian fluid, in a uniform DC electric field is investigated. Discontinuity of electrical properties such as conductivities of the internal and external fluid media as well as capacitance and conductance of the membrane lead to a net interfacial Maxwell stress which can cause the deformation of such an elastic capsule. We investigate this problem considering well established membrane laws for a thin elastic membrane, with fully resolved hydrodynamics in the Stokes flow limit and describe the electrostatics using the capacitor model. In the limit of small deformation, the analytical theory predicts the dynamics fairly satisfactorily. Large deformations at high capillary number though necessitate a numerical approach (Boundary element method in the present case) to solve this highly nonlinear problem. Akin to vesicles, at intermediate times, highly nonlinear biconcave shapes along with squaring and hexagon like shapes are observed when the outer medium is more conducting. The study identifies the essentiality of parameters such as high membrane capacitance, low membrane conductance, low hydrodynamic time scales and high capillary number for observation of these shape transitions. The transition is due to large compressive Maxwell stress at the poles at intermediate times. Thus such shape transition can be seen in spherical globules admitting electrical capacitance, possibly, irrespective of the nature of the interfacial restoring force.

## 1 Introduction

An elastic capsule can be considered to be a drop of a liquid separated from another liquid by a very thin elastic membrane [Barthès-Biesel and Rallison, 1981]. The role of such an elastic interface is not only to prevent permeation of one fluid into another, thereby preventing mixing of contents, but also maintain the integrity of the capsule. The membrane can enclose a complex functional fluid, for example, biological cells which are capsules with membranes enclosing cell organelles embedded in a thick cytoplasm. These membranes are made up of amphiphilic molecules such as lipids which form bilayers, block copolymers which can form monolayers or crosslinked surface active moieties [Karyappa et al., 2014a, Kataoka et al., 2001]. They are popular as encapsulating agents and are used as carriers for drugs, genes and other biotechnologically relevant materials [Kataoka et al., 2001].

Biologically important capsules such as Red-blood cells or capsules used in technological applications, are subject to large external forces, such as shear or electric forces, during their life-span.

These forces can cause significant deformation in the capsules resulting in membrane stresses and shape deformation. From a mechanics point of view, a membrane of an elastic capsule can be considered as a two dimensional interface, characterized by an elastic modulus, that undergoes in-plane deformation (strain) to generate in-plane elastic stresses [Barthès-Biesel and Rallison, 1981] etc. These elastic stresses resist the applied forces such that a force balance and thereby a steady shape is attained and the capsule retains its integrity. Different kinds of constitutive relationships relating in-plane finite deformation, strain measures to in-plane stresses have been developed for a variety of membrane materials having technological or biological significance. Previously used elastic solid [Lighthill, 1968] and liquid droplet models [Hyman and Skalak, 1972] have now been replaced by thin viscoelastic membrane models with properties, such as elastic and viscous moduli of the membrane, taking account of the microscopic response corresponding to the microstructure of the capsule. Among several membrane constitutive laws, the Mooney-Rivlin law [Green and Adkins, 1970] for a strain softening membrane and Skalak law [Skalak et al., 1973] for a strain hardening membrane are popularly used especially in the computational analyses of elastic capsules [Gao et al., 2001, Fery and Weinkamer, 2007, Keller and Sottos, 2006, Dubreuil et al., 2003, Chang and Olbricht, 1993].

The deformation of elastic capsules subjected to weak forces (shear or electric) have been studied using asymptotic theories that assume an expansion parameter which is typically the capillary number (a ratio of destabilizing force typically shear or electric to the stabilizing elastic force) and the deformation is assumed to be proportional to the capillary number [Barthès-Biesel and Rallison, 1981, Barthès-Biesel, 1980, Barthès-Biesel and Chhim, 1981, Barthès-Biesel, 1991, Ha and Yang, 2000, Thaokar, 2016, Kessler et al., 2009, Finken et al., 2011]. In most examples of practical relevance though, the capillary number, and thereby the deformation, can be quite high. The non-linear elastic response becomes relevant and an accurate description is possible only by a suitable numerical method.

In the last three decades, several computational studies addressing a variety of issues in large deformation problems in elastic capsules have been reported. Zhou and Pozrikidis [1995] studied the deformation of a capsule with an area incompressible membrane in simple shear flow using the boundary integral method. Such a membrane develops tension because of the imposed area incompressibility under applied shear flow. Later several other investigations reported the study on the deformation of capsules and red blood cells in shear flow and looked at aspects such as deformation under small and moderate capillary numbers (proportional to the rate of shear) Finken et al. [2011], effects of viscosity ratio on deformation as well as tumbling and tanktreading Finken et al. [2011], Rao et al. [1994], Pozrikidis [1995], Ramanujan and Pozrikidis [1998], Pozrikidis [2001], Le [2010], Kessler et al. [2008], Sui et al. [2008a], effects of initial shape of the capsule as well as membrane constitutive laws on deformation and instability beyond a critical capillary number Sui et al. [2007, 2010], Skotheim and Secomb [2007], Navot [1998]. Significant sensitivity to membrane constitutive laws has also been investigated, for example the computational studies on the deformation of a capsule with strain hardening and strain softening membrane under linear shear flow [Barthès-Biesel, 1991, Lac et al., 2004, Lac and Barthès-Biesel, 2005, Sui et al., 2008b] indicates that membrane resistance in a strain hardening capsule (obeying the Skalak law [Skalak et al., 1973]) may prevent its burst.

In the large deformation limit, the numerical analysis of elastic interfaces interacting with fluids lead to a coupled solid-fluid interaction problem, which is known to present formidable numerical challenges. For instance, elastic instabilities [Finken and Seifert, 2006, Dodson and Dimitrakopoulos, 2009] are commonly encountered in their numerical solution, thereby severely limiting analysis of large deformation problems. A membrane that offers resistance to bending can suppress these numerical elastic instabilities [Pozrikidis, 2001, Sui et al., 2007, Kwak and Pozrikidis, 2001, Dupont et al., 2015]. Several computational studies on the dynamics of elastic capsules ignore the bending resistance [Zhou and Pozrikidis, 1995, Pozrikidis, 1995, Lac et al., 2004], predominantly because the bending force depends upon the fourth derivative of the position vector, thereby introducing numerical errors. Thus, although highly relevant, a good numerical model for addressing large deformation problems remains a challenge.

The present work addresses the large deformation of capsules induced by strong uniform DC electric fields. The response of capsules to electric fields is important in biomedical applications such as electroporation [Crowley, 1973, Tieleman, 2004], electrofusion [Neumann et al., 1989], cell separation and manipulation [Pethig, 1996, Kang et al., 2008]. Moreover, the response of spherical globules such as drops, vesicles and capsules to electric field can be used to understand the interfacial properties as well as novel aspects of electrohydrodynamics [Karyappa et al., 2014a, Thaokar, 2016, Yamamoto et al., 2010, Thaokar and Deshmukh, 2010, Deshmukh and Thaokar, 2012a, 2013a, Karyappa et al., 2014b, Das et al., 2015, McConnell et al., 2015a, Ouriemi and Vlahovska, 2015]. Uniform field also implies axisymmetry in most cases, thereby allowing easy-to-analyze experiments as well as elegant analytical theory and simplified numerical models, such as using the boundary element method.

Relatively few studies have been reported on the deformation of elastic capsules under DC [Ha and Yang, 2000] and AC [Thaokar, 2016] electric fields, both restricted to small deformation limit. Experiments, small deformation theory and boundary integral calculations of a capsule, with a conducting membrane, enclosing a conducting fluid and suspended in a dielectric external fluid medium, showed that its deformation can be quite different from that of drops, and that it can be used to estimate linear and nonlinear elastic properties of the capsules [Karyappa et al., 2014a].

Experimental investigations [Yamamoto et al., 2010, Riske and Dimova, 2006, Dimova et al., 2007, 2009] on the deformation of a vesicle in a strong electric field showed squaring of the vesicle with high values of tension at the corners. This was also reaffirmed and explained by a few 2-D [McConnell et al., 2015a,b, 2013] and 3-D [Veerapaneni, 2016, Kolahdouz and Salac, 2015a,b] computational analyses. Vesicles and capsules are inherently different at least on a few counts: vesicles are area preserving, which means a spherical vesicle cannot undergo deformation. Thus a vesicle can deform only if it has an excess area, and it resists deformation via the bending forces as well as uniform and non-uniform tensions generated to conserve the area. Capsules on the other hand can resist deformation by elastic forces which arise as deviation from a reference, unstressed shape which can also be a sphere.

In this work we consider a capsule with a membrane that exhibits Skalak or neo-Hookean (a special case of Mooney-Rivlin model) membrane constitutive law along with the capacitor model for the electric field to study the dynamics of capsule deformation under strong electric field and ask the following questions: what is the response of a capsule characterized by a capacitance and

conductance to externally applied uniform DC fields, using analytical theory and Boundary integral calculations. What is the effect of these electrical properties of membrane as well as competition of the various timescales in the problem such as membrane charging time, Maxwell-Wagner relaxation time, membrane deformation time, hydrodynamic relaxation times on the deformation? Is there a possibility of squaring and other large deformation modes in elastic capsules, akin to that reported in vesicles and the necessary conditions thereof? and what are the possible breakup modes and their dependence on the type of membrane models?

## 2 Problem description

The schematic representation of a deformed elastic capsule in uniform electric field is shown in fig. 1. A uniform DC electric field is applied parallel to the  $y$  axis which is the axis of symmetry of the capsule. This field is defined by  $\tilde{\mathbf{E}}^\infty = \tilde{E}_0 \mathbf{e}_y$ , where  $\tilde{E}_0$  is the strength of the electric field and thus acts in the +ve  $y$  direction. All the notations, in this article, with a tilde ( $\sim$ ) represent dimensional quantities, whereas without ( $\sim$ ) represent their nondimensional counterpart.

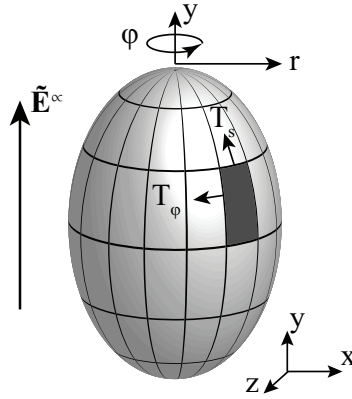


Figure 1: Schematic representation of a capsule in a uniform electric field.

The position vector, as measured from the origin is given by  $\tilde{\mathbf{x}} = \tilde{x}\mathbf{e}_x + \tilde{y}\mathbf{e}_y + \tilde{z}\mathbf{e}_z$ , where  $\mathbf{e}_x$ ,  $\mathbf{e}_y$ , and  $\mathbf{e}_z$  are the unit vectors in the  $x$ ,  $y$ , and  $z$  directions, respectively. The axis of symmetry of the capsule is assumed to coincide with the  $y$  axis, such that its centroid is at the origin. In the axisymmetric configuration (cylindrical coordinates),  $y$  is the axis of the cylindrical coordinate system, where as  $\phi$  is the azimuthal angle. The radial coordinate  $r = \sqrt{x^2 + z^2}$ . When local spherical coordinate system is used in the analytical theory, presented in the appendix,  $r = \sqrt{x^2 + y^2 + z^2}$  and the azimuthal and polar angles are  $\phi$  and  $\theta$  respectively, where  $\theta$  is measured from the  $y$  axis in the clockwise direction.  $\mathbf{n}$  and  $\mathbf{t}$  are considered to be the outward unit normal and clockwise unit tangent to the surface of the capsule, respectively. The dielectric constant and electrical conductivity of internal fluid medium are  $\epsilon_i$  and  $\sigma_i$ , respectively, whereas the external medium has a dielectric constant and an electrical conductivity given by  $\epsilon_e$  and  $\sigma_e$ , respectively. Subscripts  $i$  and  $e$  stand for internal and the external fluid media of the capsule, respectively. The ratios of electrical properties of the two media are defined as:  $\sigma_r = \sigma_i/\sigma_e$  and  $\epsilon_r = \epsilon_i/\epsilon_e$ . Both the external and the internal fluids are Newtonian, and the viscosities of the external and internal fluids are denoted by  $\mu$  and  $\lambda\mu$  respectively, where  $\lambda$  is the viscosity ratio. The mechanical properties of the membrane are elasticity,  $E_s$  and the

bending modulus,  $\kappa_b$  and the electrical properties are capacitance,  $C_m$  and conductance,  $G_m$ . The membrane is considered to be purely elastic and viscous resistance is neglected. The time is scaled by the charge relaxation time of the outer fluid,  $\tilde{t}_e = \epsilon_e \epsilon_0 / \sigma_e$ , where  $\epsilon_0$  is the permittivity of the free space and the velocity is scaled by  $E_s / \mu_e$ . The electric field ( $\tilde{\mathbf{E}}$ ), potential ( $\tilde{\phi}$ ) and the stress are scaled by  $E_0$ ,  $E_0 a$  and  $E_s / a$ . Other associated timescales in this problem are hydrodynamic response time  $\tilde{t}_H = \mu_e a / E_s$ , Maxwell-Wagner charge relaxation time  $\tilde{t}_{MW} = \epsilon_0 (\epsilon_i + 2\epsilon_e) / (\sigma_i + 2\sigma_e)$  and membrane charging time  $\tilde{t}_{cap} = a C_m (\sigma_i + \sigma_e / 2)$ . Nondimensional counterparts of all these timescales are  $t_e = 1$ ,  $t_H = \tilde{t}_H / \tilde{t}_e$ ,  $t_{MW} = \tilde{t}_{MW} / \tilde{t}_e = (2 + \epsilon_r) / (2 + \sigma_r)$  and  $t_{cap} = \tilde{t}_{cap} / \tilde{t}_e = \hat{C}_m (1/2 + 1/\sigma_r)$  where  $\hat{C}_m = a C_m / \epsilon_e \epsilon_0$  is the nondimensional membrane capacitance [Grosse and Schwan, 1992].

A balance between the Maxwell stresses caused by the electric field, the elastic forces and hydrodynamic forces result in the evolution of a capsule into a new shape. It is of interest to establish a quantitative relationship between the deformation, elasticity and the strength of the electric field. Capsule deformation is analyzed by considering neo-Hookean and Skalak type of membranes representing strain softening and hardening membranes, respectively. For modelling electric response of the capsule to the applied electric field a capacitive membrane model is used which incorporates the capacitance and conductance of the membrane as well as the contrast in conductivity and dielectric constant between the internal and external fluid media. For simplicity of computations the interface is considered to be impermeable, thereby preventing osmotic flows across the membrane. Since the elastic forces at large deformations are known to result in the formation of sharp edges and high curvatures, bending forces are included along with the elastic forces. Moreover, inclusion of resistance to bending also allows removal of spurious elastic instabilities known to occur in elastic interfaces.

### 3 Problem formulation

The deformation of an elastic capsule in uniform electric field is assumed to remain axisymmetric with the axis parallel to the electric field lines. Therefore, to study the electrohydrodynamics of capsule deformation axisymmetric boundary integral method is considered. The electric, elastic and hydrodynamic forces as well as the bending resistance of the membrane are in equilibrium at the interface for an inertialess membrane and these are discussed next.

#### 3.1 Electrostatics

The electric potentials inside and outside of the capsule satisfy the Laplace equation  $\nabla^2 \phi_{i,e} = 0$ . Therefore the electric potential can be obtained as an integral equation by using Green's theorem for the solution of the Laplace equation, to yield, [McConnell et al., 2015a,b, 2013]:

$$\frac{1}{2} \phi_i(\mathbf{x}_0) = \int_s [G^E(\mathbf{x}, \mathbf{x}_0) \nabla \phi_i(\mathbf{x}) \cdot \mathbf{n}(\mathbf{x}) - \phi_i(\mathbf{x}) \mathbf{n}(\mathbf{x}) \cdot \nabla G^E(\mathbf{x}, \mathbf{x}_0)] ds(\mathbf{x}), \quad (1)$$

$$\frac{1}{2} \phi_e(\mathbf{x}_0) = \phi^\infty(\mathbf{x}_0) - \int_s [G^E(\mathbf{x}, \mathbf{x}_0) \nabla \phi_e(\mathbf{x}) \cdot \mathbf{n}(\mathbf{x}) - \phi_e(\mathbf{x}) \mathbf{n}(\mathbf{x}) \cdot \nabla G^E(\mathbf{x}, \mathbf{x}_0)] ds(\mathbf{x}), \quad (2)$$

where  $G^E(\mathbf{x}_0, \mathbf{x}) = \frac{1}{4\pi|\mathbf{x}|}$  is the Green function for the Laplace equation,  $\phi^\infty = -y$  is the applied potential ( $\tilde{\phi}^\infty = -E_0 \tilde{y}$ ).

The transmembrane potential, defined as the discontinuity in electrical potential across the in-

interface, is given by

$$\phi_m = \phi_i - \phi_e \quad (3)$$

and it can be calculated from the electrical current continuity (a sum of displacement and Ohmic currents) in the direction normal to the plane of the membrane [DeBruin and Krassowska, 1999]

$$\sigma_r E_{n,i} + \epsilon_r \frac{dE_{n,i}}{dt} = E_{n,e} + \frac{dE_{n,e}}{dt} = \hat{C}_m \frac{d\phi_m}{dt} + \hat{G}_m \phi_m, \quad (4)$$

where  $E_{n,i}$  and  $E_{n,e}$  are normal electric fields at inside and outside of be membrane and  $\hat{G}_m = aG_m/\sigma_e$  is the nondimensional membrane conductance. Solving section 3.1 along with eq. (3) and eq. (4), the tangential (derivative of potential with respect to the arc-length) and normal electric fields can be calculated (termed as boundary integral method with capacitor model, BEM-CM).

The discontinuity of the electric traction across the interface is given by  $\mathbf{f}^E = (\tilde{\tau}_e^E - \tilde{\tau}_i^E) \cdot \mathbf{n} = \tilde{\tau}_n^E \mathbf{n} + \tilde{\tau}_t^E \mathbf{t}$ , where the dimensional Maxwell electric stress  $\tilde{\tau}^E = \epsilon \epsilon_0 (\tilde{\mathbf{E}}\tilde{\mathbf{E}} - \frac{1}{2}\tilde{E}^2 \mathbf{I})$ , considering  $\mathbf{I}$  as the identity tensor and  $\epsilon$  as the dielectric constant of the fluid. The normal and tangential components of the electric stress tensor can be expressed in nondimensional form as

$$\tau_n^E = \frac{1}{2}Ca [(E_{n,e}^2 - E_{t,e}^2) - \epsilon_r(E_{n,i}^2 - E_{t,i}^2)], \quad (5)$$

$$\tau_t^E = Ca (E_{n,e}E_{t,e} - \epsilon_r E_{n,i}E_{t,i}), \quad (6)$$

where  $Ca = a\epsilon\epsilon_0 E_0^2/E_s$  is the ratio of the electric force to the elastic force.

### 3.2 Membrane laws and elastic stress

For an isotropic and area dilating membrane, elastic tensions can be calculated using the Mooney Rivlin model [Green and Adkins, 1970]. According to the Mooney-Rivlin law, the membrane tension in the principal direction  $i$  can be expressed as

$$\tilde{T}_i^{MR} = \frac{\tilde{G}_{MR}}{\lambda_i \lambda_j} \left( \lambda_i^2 - \frac{1}{\lambda_i^2 \lambda_j^2} \right) [\alpha + \lambda_j^2 (1 - \alpha)], \quad (7)$$

where  $G^{MR}$  and  $\alpha$  are the surface elastic modulus and measure of the nonlinearity of the Mooney-Rivlin law, respectively and  $\lambda_{i,j}$  are stretch ratios in principal directions  $i$  and  $j$ . Membrane nonlinearity parameter  $\alpha$  varies in a range of  $[0, 1]$ , a special case corresponding to  $\alpha = 1$  is termed as neo-Hookean law which is used in this work [Barthès-Biesel et al., 2002].

The relation between the non-dimensional membrane elastic tensions and the stretch ratios for a strain hardening membrane in the principal direction  $i$  is given by Skalak et al. [1973]

$$\tilde{T}_i^{SK} = \frac{\tilde{G}^{SK}}{\lambda_i \lambda_j} [\lambda_i^2 (\lambda_i^2 - 1) + C (\lambda_i \lambda_j)^2 \{ (\lambda_i \lambda_j)^2 - 1 \}], \quad (8)$$

where the first term at the right hand side accounts for the shear deformation associated with the modulus  $G^{SK}$  and the second term accounts for the area dilatation with the modulus  $CG^{SK}$ . The area dilatation parameter  $C$  controls the extent of change in area, higher the value of  $C$  lower is the membrane dilatation, a small value of  $C = 1$  is chosen to allow the membrane to change its area dur-

ing deformation. Membrane tension in the principal direction  $j$  can be expressed by interchanging indices in the corresponding constitutive relations (eq. (7) and eq. (8)). In our consideration  $i$  is the meridional and  $j$  is the azimuthal principal directions and the corresponding tensions are considered as  $T_s$  and  $T_\phi$ . In the small deformation limit,  $G^{MR}$  and  $G^{SK}$  are related to the surface Young modulus,  $E_s$ , [Barthès-Biesel et al., 2002] as  $E_s = 3G^{MR} = 2G^{SK}(1 + 2C)/(1 + C)$ .

A combined contribution of the elastic tensions (force/length) obtained from the constitutive laws govern the membrane elastic traction (force/area), given by  $\mathbf{f}^{el} = \tau_n^{el} \mathbf{n} + \tau_t^{el} \mathbf{t}$ , exerted at the interface. The components of the elastic stresses can be obtained as

$$\tau_n^{el} = -(K_s T_s + K_\phi T_\phi) \quad (9)$$

$$\tau_t^{el} = \frac{dT_s}{ds} + \frac{1}{r} \frac{dr}{ds} (T_s - T_\phi) \quad (10)$$

where  $K_s = \left| \frac{d\mathbf{t}}{ds} \right|$  and  $K_\phi = \frac{n_r}{r}$  are principal curvatures of the meridional surface.  $t_y = n_r = \frac{dy}{ds}$  and  $t_r = -n_y = \frac{dr}{ds}$  are the  $y$  and  $r$  components of the unit normal and tangent vectors at the interface, respectively.

### 3.3 Resistance due to bending

Even though thin elastic membranes have very low resistance to bending deformations, it can have significant contribution to the restoring forces especially at the regions of high curvature. The overall dimensionless bending force (force/area) is given by

$$\mathbf{f}^b = \hat{\kappa}_b [2\Delta_s H + 4H(H^2 - K_G)] \mathbf{n}, \quad (11)$$

where  $H$  and  $K_G$  are the mean curvature ( $H = \frac{1}{2}(K_s + K_\phi)$ ) and Gaussian curvature ( $K_G = K_s K_\phi$ ), respectively and the nondimensional bending rigidity,  $\hat{\kappa}_b = \kappa_b/a^2 E_s$  is the ratio of the bending force to the elastic force.  $\Delta_s H$  is the Laplace Beltrami of the mean curvature in cylindrical coordinate system, defined as

$$\Delta_s H = \nabla_s \cdot (\nabla_s H) = \frac{1}{r |\mathbf{X}_s|} \frac{\partial}{\partial s} \left( \frac{r}{|\mathbf{X}_s|} \frac{\partial H}{\partial s} \right), \quad (12)$$

where  $|\mathbf{X}_s| = \sqrt{\frac{\partial r^2}{\partial s^2} + \frac{\partial y^2}{\partial s^2}}$  [Hu et al., 2014]. Higher order derivatives of mean curvature with respect to arc length are calculated using spectral method for better accuracy in estimating bending force.

### 3.4 Hydrodynamics

Typically capsule sizes range from 0.1 to few hundreds of microns which means that the flow inside and outside the interface can be considered to obey low Reynolds number hydrodynamics and therefore the Stokes equations suffice to describe the problem. Thus

$$\nabla \cdot \mathbf{u} = 0, \quad \nabla \cdot \boldsymbol{\tau}^H = 0, \quad (13)$$



where viscous stress for the internal fluid domain  $V$  and external fluid domain  $V^*$  are given by

$$\boldsymbol{\tau}^{\mathbf{H}} = -P\mathbf{I} + \lambda(\nabla\mathbf{u} + \nabla\mathbf{u}^T) \quad \text{at } V, \quad (14)$$

$$\boldsymbol{\tau}^{\mathbf{H}} = -P\mathbf{I} + (\nabla\mathbf{u} + \nabla\mathbf{u}^T) \quad \text{at } V^*, \quad (15)$$

where  $\boldsymbol{\tau}^{\mathbf{H}}$  is the hydrodynamic stress tensor,  $\mathbf{u}$ , and  $P$  are the velocity and pressure fields, respectively.

The solution to eq. (13) results in the interfacial velocity to be described in an integral form as

$$\mathbf{u}(\mathbf{x}_0) = -\frac{1}{1+\lambda} \frac{1}{4\pi} \int_s \Delta\mathbf{f}(\mathbf{x}) \cdot \mathbf{G}(\mathbf{x}_0, \mathbf{x}) ds(\mathbf{x}) - \frac{1}{4\pi} \frac{1-\lambda}{1+\lambda} \int_s \mathbf{u}(\mathbf{x}) \cdot \mathbf{Q}(\mathbf{x}_0, \mathbf{x}) \cdot \mathbf{n}(\mathbf{x}) ds(\mathbf{x}), \quad (16)$$

where  $\mathbf{G}(\mathbf{x}_0, \mathbf{x})$  and  $\mathbf{Q}(\mathbf{x}_0, \mathbf{x})$  are Green's functions for velocity (stokeslet) and stress (stresslet) respectively and  $\Delta\mathbf{f}$  is the unbalanced non-hydrodynamic traction acting on the interface [Rallison and Acrivos, 1978]. For an unbounded three dimensional flow, the stokeslet and the stresslet are defined as,

$$\mathbf{G}(\mathbf{x}_0, \mathbf{x}) = \frac{\mathbf{I}}{|\hat{\mathbf{x}}|} - \frac{\hat{\mathbf{x}}\hat{\mathbf{x}}}{|\hat{\mathbf{x}}|^3}, \quad Q_{ijk}(\mathbf{x}_0, \mathbf{x}) = -6 \frac{\hat{\mathbf{x}}\hat{\mathbf{x}}\hat{\mathbf{x}}}{|\hat{\mathbf{x}}|^5} \quad \text{where } \hat{\mathbf{x}} = \mathbf{x} - \mathbf{x}_0, \quad (17)$$

where  $\mathbf{x}_0$  and  $\mathbf{x}$  are the source point and the observation point, respectively. The viscosity of the two fluids is assumed to be the same, i.e.  $\lambda = 1$ , whereby the double layer potential, second term in the right hand side of eq. (16), drops out. The boundary integral equation (eq. (16)) is solved to obtain the interfacial velocity of an axisymmetric deformable body, capsule, in applied uniform electric field [Karyappa et al., 2014a, Deshmukh and Thaokar, 2012b, 2013b, Pozrikidis, 1990]. The non-hydrodynamic tractions responsible for the deformation of capsule, in this case, include the elastic traction, electric traction and traction due to the resistance to bending. The net non-hydrodynamic traction acting at the interface is given by

$$\Delta\mathbf{f} = \mathbf{f}^{el} + \mathbf{f}^E + \mathbf{f}^b. \quad (18)$$

Eventually, the deformed shape of the capsule,  $\mathbf{x}(t)$ , can be calculated from the kinematic condition given by

$$\mathbf{x}(t) = \mathbf{x}(t-1) + \frac{1}{t_H} \mathbf{u} \Delta t, \quad (19)$$

where  $\mathbf{x}(t-1)$  is the shape of the capsule at previous time,  $(t-1)$ ,  $\Delta t$  is the time step used in boundary integral calculation.

## 4 Results

Results are presented for the dynamics of axisymmetric deformation of an elastic capsule, placed in a uniform DC electric field, by considering membrane conductance  $\hat{G}_m = 0$ , capacitance  $\hat{C}_m = 50$ , ratio of dielectric constant  $\epsilon_r = 1$  and the hydrodynamic response time  $t_H = 1$ , unless explicitly mentioned. Assuming very small contribution of the resistance due to bending, a small value of dimensionless rigidity modulus  $\kappa_b = 0.001$  is considered and the criticality of incorporating bending is clearly demonstrated in section A.4. Axisymmetric boundary integral method is used to sim-



ulate in which the azimuthal elliptic integrals are solved using analytical theory and integrations in meridional plane are carried out numerically using 16–point Gaussian quadrature considering 60-collocation points over the arc length between poles (north - south).

#### 4.1 Validation of the numerical code

The deformation of an elastic capsule in electric field can be analytically solved in the small capillary number limit. Steady state deformation obtained from boundary integral method for a neo-Hookean membrane and a Skalak membrane are compared (fig. 2) with the results obtained from simplified electrostatic theory (SEM) (section A.1.2) considering  $\hat{C}_m = 50$ ,  $\hat{G}_m = 0$ ,  $\varepsilon_r = 1$  and  $\sigma_r = 1$ , (although it does not depend upon  $\sigma_r$  which is discussed in section 4.2.3). It can be observed that the deformations considering neo-Hookean and Skalak membrane law are in good agreement with the analytical theory in the small deformation limit and both kind of membranes exhibit same degree of deformation which in turn is identical to that given by a Hookean membrane. A deviation is observed at higher capillary numbers because of corrections to both electrostatics as well as elastic deformation.

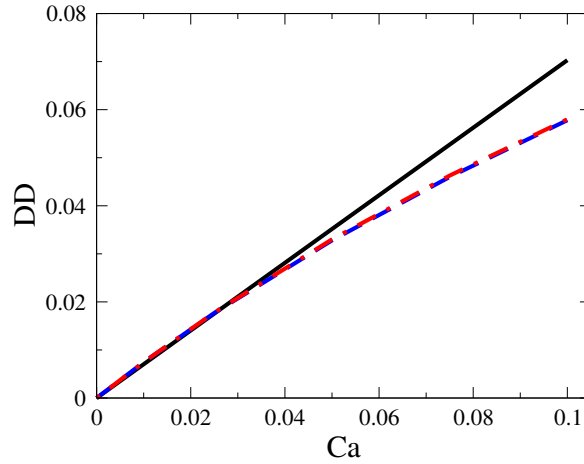


Figure 2: Comparison of degree of deformation as a function of  $Ca$  obtained from analytical theory (—), boundary integral simulation considering simplified electrostatic model with Skalak law (---) and neo-Hookean law (---) considering  $\hat{C}_m = 50$ ,  $\hat{G}_m = 0$ ,  $\varepsilon_r = 1$  and  $\sigma_r = 1$ .

Numerical boundary integral method to solve the electrostatics is further validated with the analytical electrostatics theory (AET), discussed in section A.1.1, which essentially solves electrostatics equations over an undeformed sphere (figs. 20a to 20c, 21a to 21c and 22a to 22c in section A.2). Analytical theory for deformation though is not provided in this limit owing to complicated expressions. It should be mentioned here that in the analytical theory as well as in the numerical model, the choice of initial condition on the inner and outer electric field is critical, and is a characteristic of the capacitor model. In this work, we assume that the non-dimensional inner and outer normal electric field at  $t = 0$  is given by  $\cos \theta$ . This pre-supposes that the capacitor is uncharged at  $t = 0$ , and offers no impedance, thereby the two fluids which have the same dielectric constants (as assumed in this work) have the same initial electric fields.

A simplified electrostatics model (SEM) is also suggested (section A.1.2) by assuming that the Maxwell-Wagner charge relaxation times is much smaller than the capacitor charging time i.e

$t_{MW} < t_{cap}$ . In this limit though, analytical solution for the deformation of a capsule is obtained and compared with numerical computations (figs. 23a to 23c in section A.2). The variation of transmembrane potential obeys  $\phi_m = \frac{3}{2}(1 - e^{-t/t_{cap}}) \cos \theta$ , which suggests that the charging time is proportional to capacitance and equal to  $3\hat{C}_m/2$  for  $\sigma_r = 1$  [Grosse and Schwan, 1992, Schwalbe et al., 2011]. The membrane becomes fully charged at long times with equal and opposite non-dimensional charge densities on either sides of the membrane (equal to  $3\hat{C}_m/2$ ) such that the net charge is zero.

## 4.2 Dynamics of capsule deformation at small and intermediate capillary numbers

The dynamics of deformation of spherical capsules with Skalak or a neo-Hookean membrane at  $\sigma_r = 1, 10$  and  $0.1$  is shown in fig. 3. These results are obtained using boundary integral calculations considering  $\epsilon_r = 1$ ,  $\hat{C}_m = 50$  and  $\hat{G}_m = 0$  at a small capillary number,  $Ca = 0.25$ . The distinctive behavior of the dynamics at different conductivity ratios and for two different membrane types are explained in the following subsections.

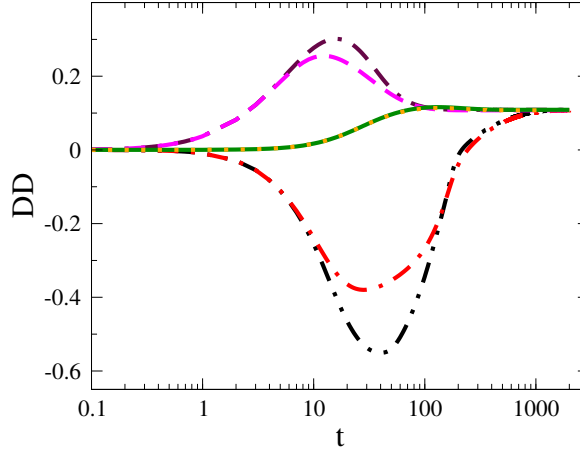


Figure 3: Dynamics for the deformation of a capsule with Skalak membrane at  $\sigma_r = 10$ ,  $\sigma_r = 1$  and  $\sigma = 0.1$  are shown by curve with line-style (---), (· · ·) and (- · -), respectively where as the deformation for a capsule with neo-Hookean membrane at  $\sigma_r = 10$ ,  $\sigma_r = 1$  and  $\sigma = 0.1$  are shown by curve with line-style (—), (— · —) and (— · ·), respectively at  $Ca = 0.25$ .

### 4.2.1 Case of $\sigma_r = 1$

For  $\sigma_r = 1$ , the deformation of a spherical capsule with either a Skalak or a neo-Hookean membrane attains an intermediate maximum prolate deformation at  $t = 132$  and slowly reaches a steady state deformation at  $Ca = 0.25$  considering  $\epsilon_r = 1$ ,  $\hat{C}_m = 50$  and  $\hat{G}_m = 0$  (fig. 3). Both Skalak and neo-Hookean capsule show nearly identical dynamics of deformation. Although there is no dielectric constant or conductivity contrast between the internal and external fluids, a steady state prolate deformation is observed. The normal electric fields are identical in the two fluids at all times, the tangential field though is discontinuous, such that the external fluid has higher magnitude than the inner fluid owing to the transmembrane potential. At  $t=0$ , the normal (outward) and tangential fields (anticlockwise) are equal for both internal and external fluids on account of same conductivities and dielectric constants and hence no net Maxwell stress is generated and the deformation is absent. As time progresses the normal electric field falls to zero, over the membrane charging time, since

at long times a fully charged non conducting membrane leads to zero current. The tangential field on the other hand continues to be negative (anti-clockwise), with the inner field always lower than the outer and the difference between the two being proportional to the transmembrane potential. At long times, the inner tangential field is zero and the outer is  $-3/2 \sin \theta$ , corresponding to the transmembrane potential (fig. 20a in section A.2). Thus, the normal Maxwell's stresses arise purely due to the tangential field (normal stress is proportional to  $E_n^2 - E_t^2$ , and  $E_n$  is same in the inner and outer surface). Therefore the normal stresses are always compressive, since the tangential electric field on the outer surface is always higher (fig. 20b in section A.2). The net normal compressive stress can be written as an isotropic compressive part and a tensile part corresponding to the 2<sup>nd</sup> Legendre polynomial of  $\cos \theta$ . This tensile part leads to prolate deformation. The tangential stresses are zero at  $t = 0$ , and  $t = \infty$ , because of absence of electric contrast, and normal electric fields being zero, respectively. The tangential stresses are from equator to pole at intermediate times.

#### 4.2.2 Case of $\sigma_r > 1$

Figure 3 shows that for  $\sigma_r = 10$  the capsule initially undergoes a high prolate deformation and then it slowly relaxes back to a steady state prolate shape. At very short times  $t < t_{MW}$ , the two fluids act as dielectrics, and since there is no dielectric contrast, the deformation is zero. The two fluids act as leaky dielectrics at time  $t \sim O(t_{MW})$  and their conductivity ratio determines their deformation, and increases as  $\sigma_r$  increases. The membrane impedance is small since  $t_{MW} < t_{cap}$ , and the membrane is not charged. Therefore, the electric field distribution as well as the Maxwell's stresses are similar to that observed in a liquid drop suspended in an ambient fluid and subjected to an electric field. The current continuity condition means that when the inner fluid is more conducting ( $\sigma_r = 10$ ), the polarization vector inside the drop is aligned in the direction of electric field, whereby there are net positive charges at the north pole and net negative charges at the south pole. Thus, unlike the  $\sigma_r = 1$  case, even the normal field contributes to normal stresses and the normal stresses are predominantly tensile (figs. 21a to 21c in section A.2), hence a strong prolate deformation is observed. At  $t > t_{cap}$ , normal electric stress at poles and tangential stress over the interface disappear as the membrane becomes fully charged. Therefore the prolate steady state deformation is mainly due to the compressive electric stress which is maximum at the equator (figs. 21a to 21c in section A.2). Note that prolate deformation is observed even in the absence of conductivity contrast as discussed earlier for  $\sigma_r = 1$  and later elaborated for the case of  $\sigma_r < 1$ .

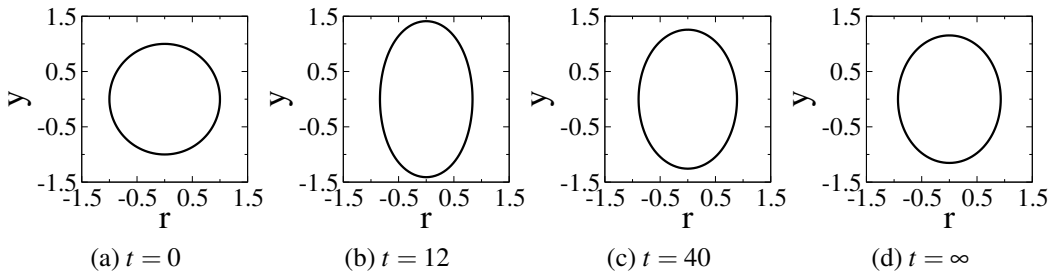


Figure 4: Shape evolution of a capsule with Skalak membrane at  $\sigma_r = 10$  for  $Ca = 0.25$ .

Intermediate shapes in the dynamics of the deformation of an elastic capsule from an initial

spherical shape to the final steady state shape at  $Ca = 0.25$  are shown in fig. 4 for  $\sigma_r = 10$ . A spherical capsule undergoes an intermediate maximum prolate deformation (fig. 4b) before reaching to the steady state deformation (fig. 4d).

#### 4.2.3 Case of $\sigma_r < 1$

When the external fluid is more conducting ( $\sigma_r = 0.1$ ), at short times, the polarization vector is from north pole to south pole, opposite in direction to the applied field, that is the north pole has a net negative charge and the south pole has a net positive charge. Thus for  $t \sim O(t_{MW})$ , the net Maxwell stress at the membrane interface is compressive and leads to an oblate shape. Note that the normal electric field leads to a compressive normal stress, and the isotropic electric pressure is also compressive (see figs. 22a to 22c in section A.2 for variation of transmembrane potential, normal and tangential electric stresses with time on a static sphere).

Interestingly, irrespective of the conductivity ratio, the final steady state deformations are the same, and are prolate (fig. 3). This independence of the final steady state shape and deformation with respect to  $\sigma_r$  can be easily understood: since at long times the nonconducting membrane acts like a dielectric, thereby rendering the outer normal electric field zero as well as the corresponding tangential stress also zero (figs. 20c, 21c and 22c in section A.2). The Maxwell stress is, therefore, only normal. Moreover, since the normal electric field is zero, the normal electric stress is compressive (figs. 20b, 21b and 22b in section A.2) and is maximum at the poles, the deformation is always prolate.

Thus a oblate-prolate transition is observed at long times for  $\sigma_r < 1$ . The exact expression although complicated, the physics seems to be governed by the normal Maxwell's stress going to zero, which in the case of SEM, leads to

$$t \propto t_{cap} \log \frac{\sigma_r + 2\sqrt{2 - \sigma_r^2}}{(2 + \sigma_r)}. \quad (20)$$

This leads to a value of around  $t = 173$  for  $\sigma_r=0.1$  which is of the same order as  $t = 243$  seen in figure figs. 3 and 5a. Thus the transition time can be expected to be of this order, although not exactly since it also depends on the capillary number as well as on the ratio of hydrodynamic and electric timescales.

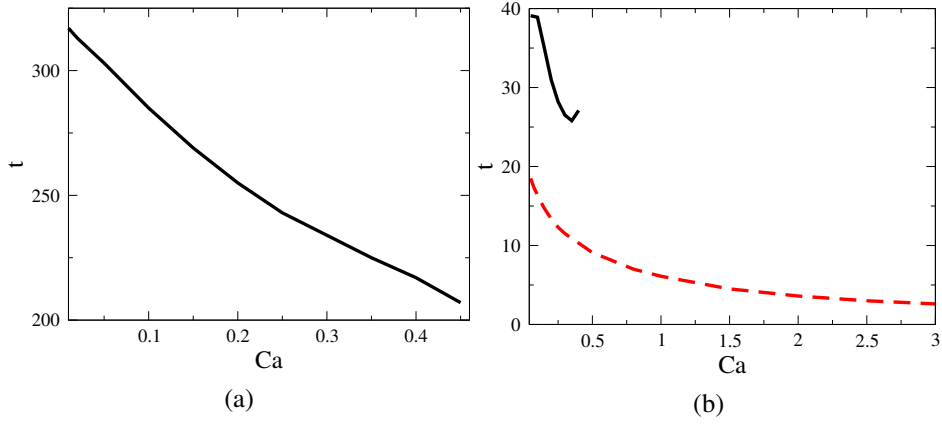


Figure 5: (a) Time required for oblate to prolate shape transition as a function of capillary number at  $\sigma_r = 0.1$ . (b) Time required to attain intermediate maximum deformation at  $\sigma_r = 10$  (—) and  $\sigma_r = 0.1$  (—).

The Skalak and the neo-Hookean models do not show much difference for  $\sigma_r > 1$ , but show significant differences in the maximum deformation for  $\sigma_r < 1$  and expectedly the strain softening neo-Hookean model shows higher deformation than the Skalak model. The time required to reach the maximum deformation is a complex interplay of the membrane charging and the fluids charging time scales, that is  $t_{MW}$  and  $t_{cap}$  and is found to obey  $t_{MW} < t < t_{cap}$ . Thus it is higher for  $\sigma_r = 0.1$  as compared to that for  $\sigma_r = 10$ . The time required to reach the maximum deformation decreases with an increase in the capillary number (fig. 5b) since typically the deforming forces are larger than the restoring forces. For  $\sigma_r = 0.1$ , at high capillary number an increase in the time required to reach the maximum deformation is observed which is essentially due to the formation of biconcave intermediate shapes (discussed later).

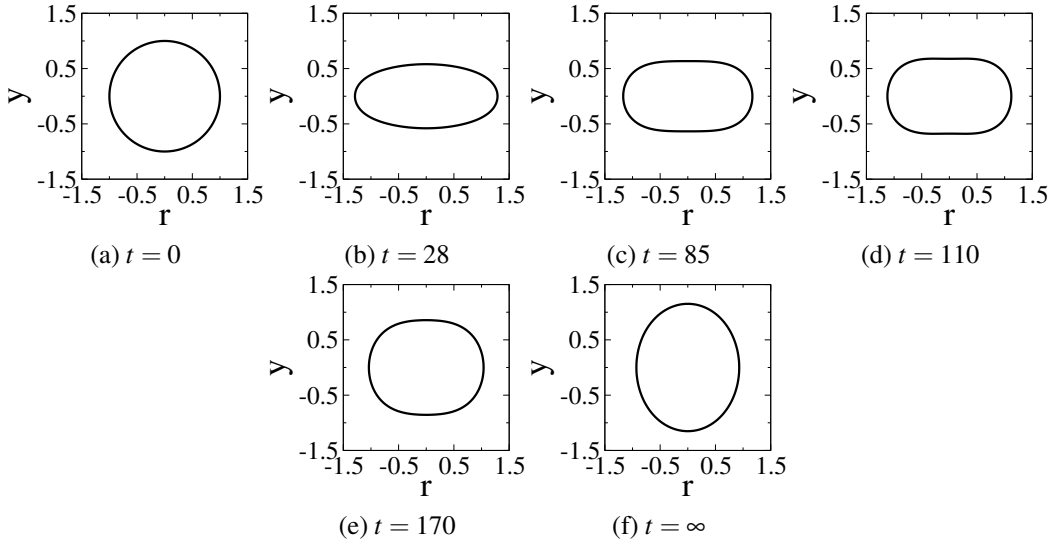


Figure 6: Shape evolution of a capsule with Skalak membrane at  $\sigma_r = 0.1$  for  $Ca = 0.25$ .

Intermediate shapes for the dynamics of the deformation of an elastic capsule from a spherical shape to the steady state shape at  $Ca = 0.25$  are shown in fig. 6 for  $\sigma_r = 0.1$ . For  $\sigma_r > 1$  prolate shapes are observed whereas oblate shapes are seen (figs. 6b to 6d) for  $\sigma_r < 1$  until the membrane

is fully charged. To understand this better, deformation studies at a still higher capillary number ( $Ca=0.45$ ) are conducted with an emphasis on  $\sigma_r < 1$ .

### 4.3 Dynamics of capsule deformation at large capillary number

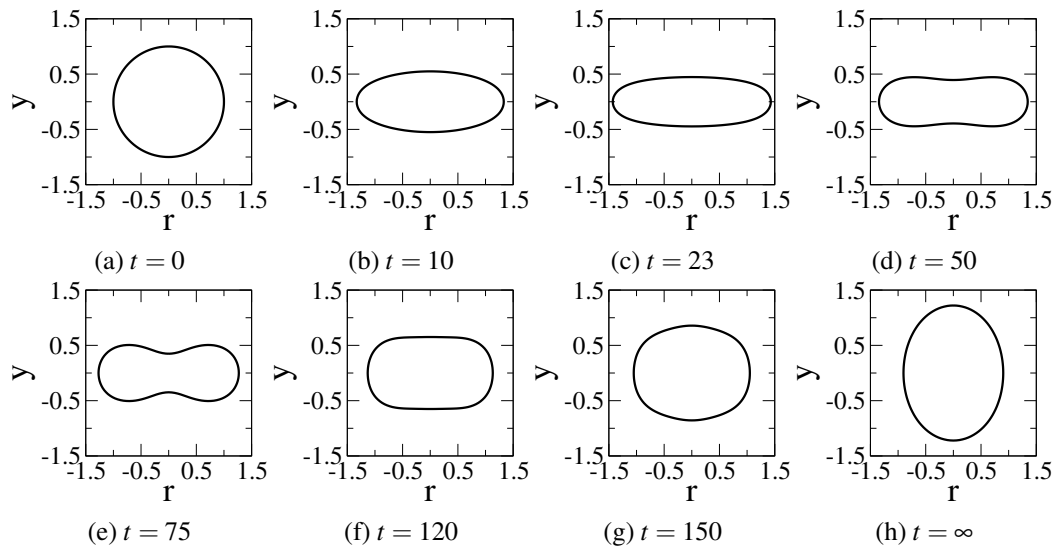


Figure 7: Shape evolution of a capsule with Skalak membrane at  $\sigma_r = 0.1$  for  $Ca = 0.45$ .

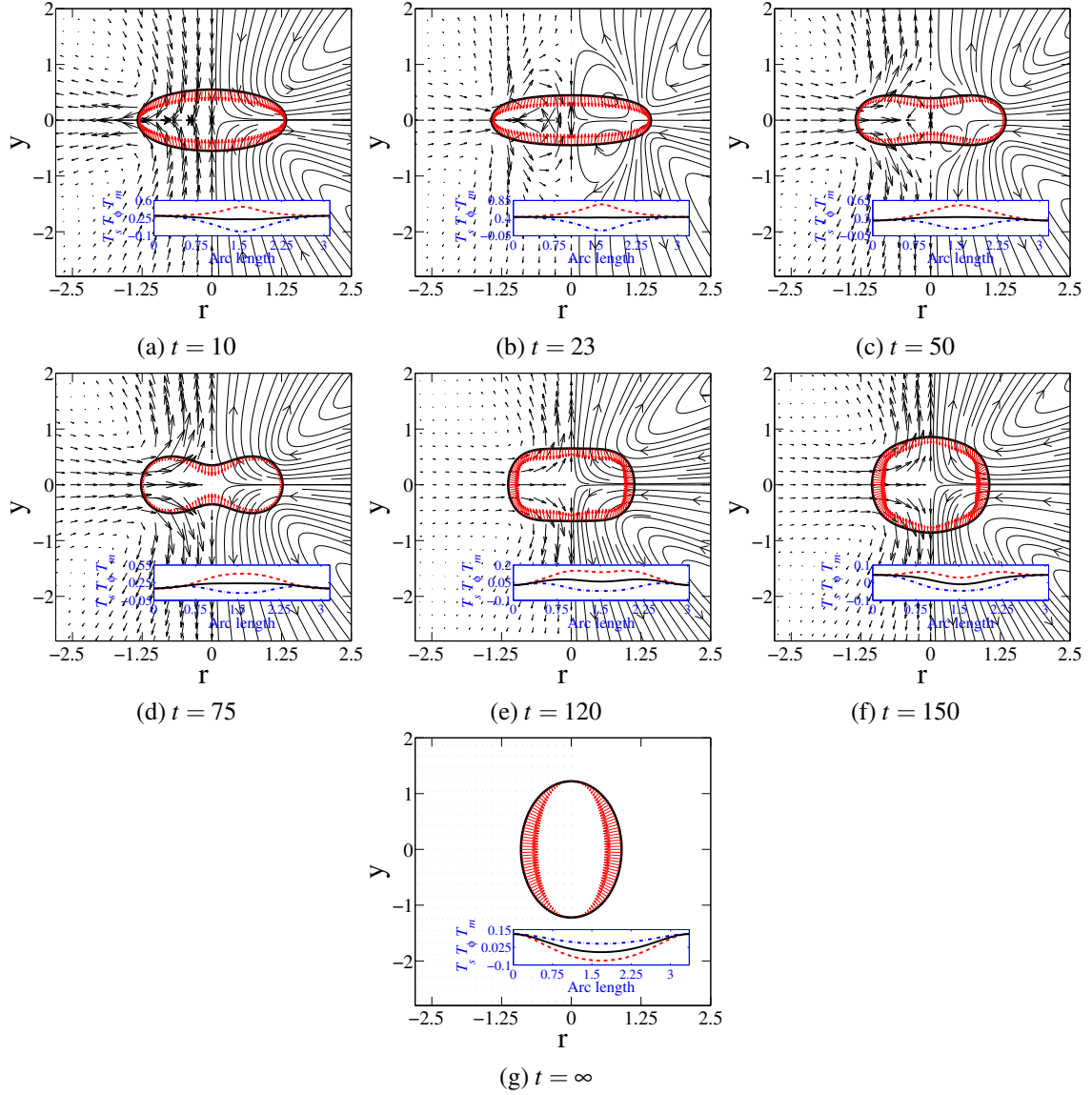


Figure 8: Stream line plot (curves with arrow, shown only at right side of axis of symmetry), velocity profile (short arrows, magnitude represents extend of flow, shown only at left side of axis of symmetry) and electric stress (arrows from the interface) for  $Ca = 0.45$  and  $\sigma_r = 0.1$  at different times. Inset shows the variation of meridional,  $T_s$  (— · —), azimuthal,  $T_\phi$  (— —) and mean,  $T_m$  (—) membrane tensions along the arc length.

The temporal evolution of a spherical capsule with  $\sigma_r = 0.1$  at a high capillary number, ( $Ca = 0.45$ ), is shown in fig. 7. In figs. 8a to 8g electric tractions, streamlines, velocity profiles are shown for figs. 7b to 7h, respectively, and meridional elastic tension ( $T_s$ ), azimuthal elastic tension ( $T_\phi$ ) and mean elastic tension ( $T_m = (T_s + T_\phi)/2$ ) are shown in the insets of figs. 8a to 8g, same data for  $Ca = 0.25$  and  $\sigma_r = 0.1$  corresponding to figs. 6b to 6f are shown in a sequence of figs. 9a to 9e.

Figure 8a shows that the oblate shape at  $\sigma_r = 0.1$  is associated with compressive normal Maxwell's stress such that their distribution is of the 2<sup>nd</sup> Legendre kind, the flow is from poles to equator due to tangential stresses, thereby assisting formation of oblate shapes. (The elastic tensions (meridional and azimuthal) are tensile for oblate shapes at short times, whereas for biconcave, squaring and hexagonal shapes observed at intermediate times the meridional tension is compressive at the equator while the azimuthal tension remains tensile. For the steady state prolate deformation, com-



pressive azimuthal tension at the equator and tensile meridional tension over the entire arc length are observed.)

Figure 8b shows further increase in the oblate deformation of the capsule because the normal Maxwell's stresses are compressive such that they are maximum at the poles and minimum at the equator. However, importantly, an onset of flow reversal (flow from equator to poles) is observed. A complex interplay of flow induced by both Maxwell stress as well as the elastic stress due to relaxation of the stretched capsule (indicated by the meridional tension also becoming tensile at the equator) leads to an initiation of biconcave shape formation of the capsule as shown in fig. 8c.

At  $t = 75$ , for  $Ca=0.45$ , although the flow is from equator to poles, the large compressive normal Maxwell stress at the poles continues to bring together the poles, resulting in a biconcave shape (fig. 8d). The biconcave shape is necessary to generate enough curvature so that the elastic stresses can balance the electric stress. On the other hand, for  $Ca=0.25$ , the compressive Maxwell stresses at poles are not high enough to cause a biconcave shape.

For  $Ca = 0.45$ , at  $t = 120$  the charging of the membrane leads to substantial compressive stress at the equator, with a corresponding lowering of stress at the poles, which results in further squaring of the capsule (fig. 8e). This is indicated by a greater region of high azimuthal tension around the equator. A peak in the azimuthal tension is now seen at the shoulders. The depression of the biconcave shape relaxes since the normal Maxwell stress at the poles reduce. The relaxation of the poles continues at  $t=150$ , leading to hexagonal shapes (fig. 8f). The shoulders seem to get arrested, probably due to the absence of electric stress, such that at  $t = \infty$  the electric stresses are compressive, which as discussed earlier, can be decomposed into an isotropic part and a tensile  $P_2(\cos \theta)$  part which disappears at  $54^\circ$ , resulting in a prolate shape (fig. 8g). In the case of  $Ca=0.25$  though, the insufficient compressive electrical stresses at the poles lead to an absence of biconcave and hexagonal shapes. This results in oblate shapes directly transforming into square shapes wherein high compressive electrical stresses at the equator as compared to poles, leads to relaxation to a prolate steady state shape.

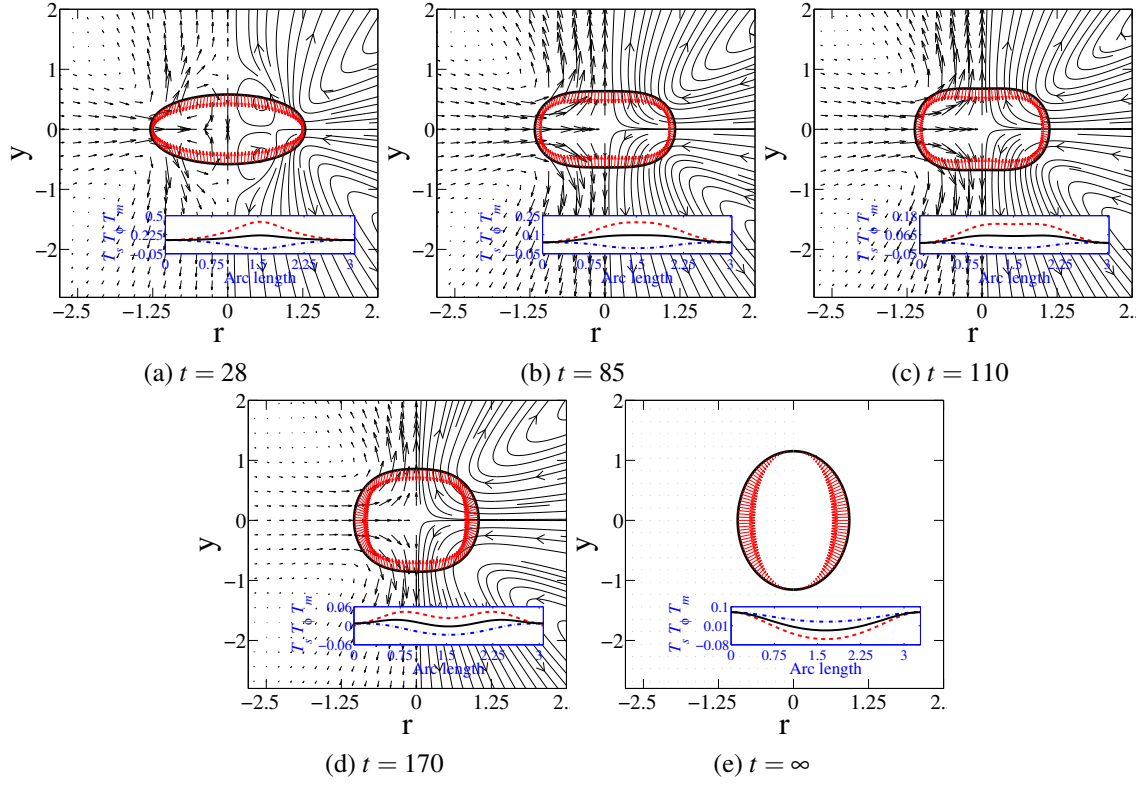


Figure 9: Stream line plot (curves with arrow, shown only at right side of axis of symmetry), velocity profile (short arrows, magnitude represents extend of flow, shown only at left side of axis of symmetry) and electric stress (arrows from the interface) for  $Ca = 0.25$  and  $\sigma_r = 0.1$  at different times. Inset shows the variation of meridional,  $T_s$  ( $-\cdot-$ ), azimuthal,  $T_\phi$  ( $---$ ) and mean,  $T_m$  ( $—$ ) membrane tensions along the arc length.

#### 4.3.1 Case of $\sigma_r > 1$

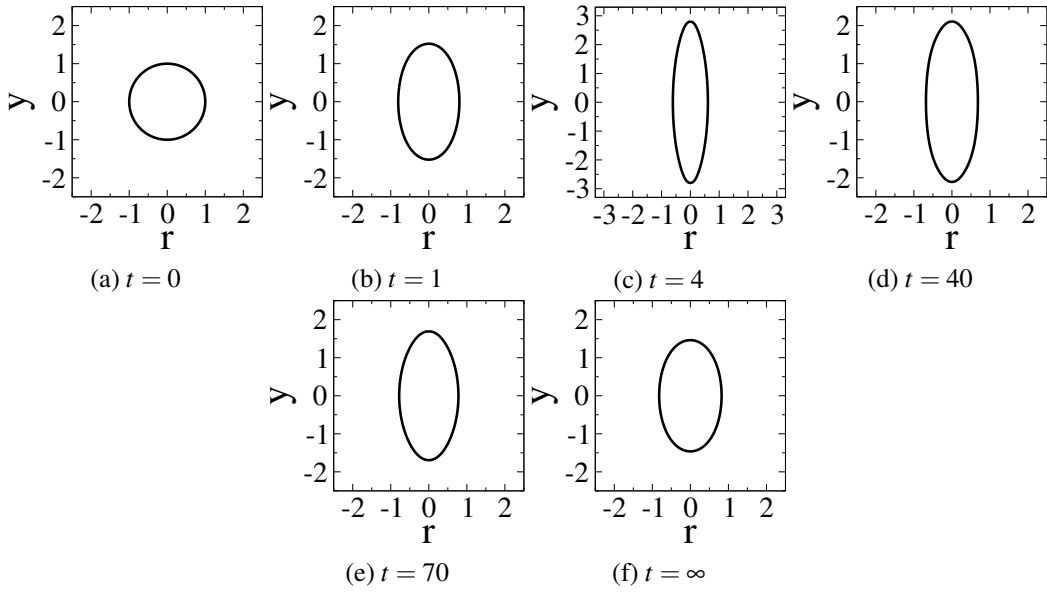


Figure 10: Shape evolution of a capsule with Skalak membrane at  $\sigma_r = 10$  for  $Ca = 2$ .

In fig. 10 the dynamics of a spherical capsule with a Skalak membrane at high capillary number ( $Ca = 2$ ) for  $\sigma_r = 10$  is shown. Unlike the case for  $\sigma_r = 0.1$ , and as discussed earlier, a capsule does not attain oblate intermediate shapes for  $\sigma_r = 10$ . Initially because of high tensile electric traction, a capsule exhibits large prolate deformation (figs. 11a and 11b). Eventually because of the compressive electric tractions at long times, it relaxes back to a steady state prolate shape (figs. 11d and 11e). At short times, the meridional and azimuthal tensions are tensile. While the meridional tension is maximum at the equator and smallest at the poles (figs. 11a and 11b), it is vice-versa for the azimuthal tension. At intermediate times, azimuthal tension is negligible around the equatorial region. At steady state, the elastic tensions are similar to that at  $\sigma_r = 0.1$ . Simultaneously, the flow changes from equator to poles at short time (fig. 11a), to poles to equator at intermediate times (figs. 11b to 11d), eventually disappearing at long times (fig. 11e).

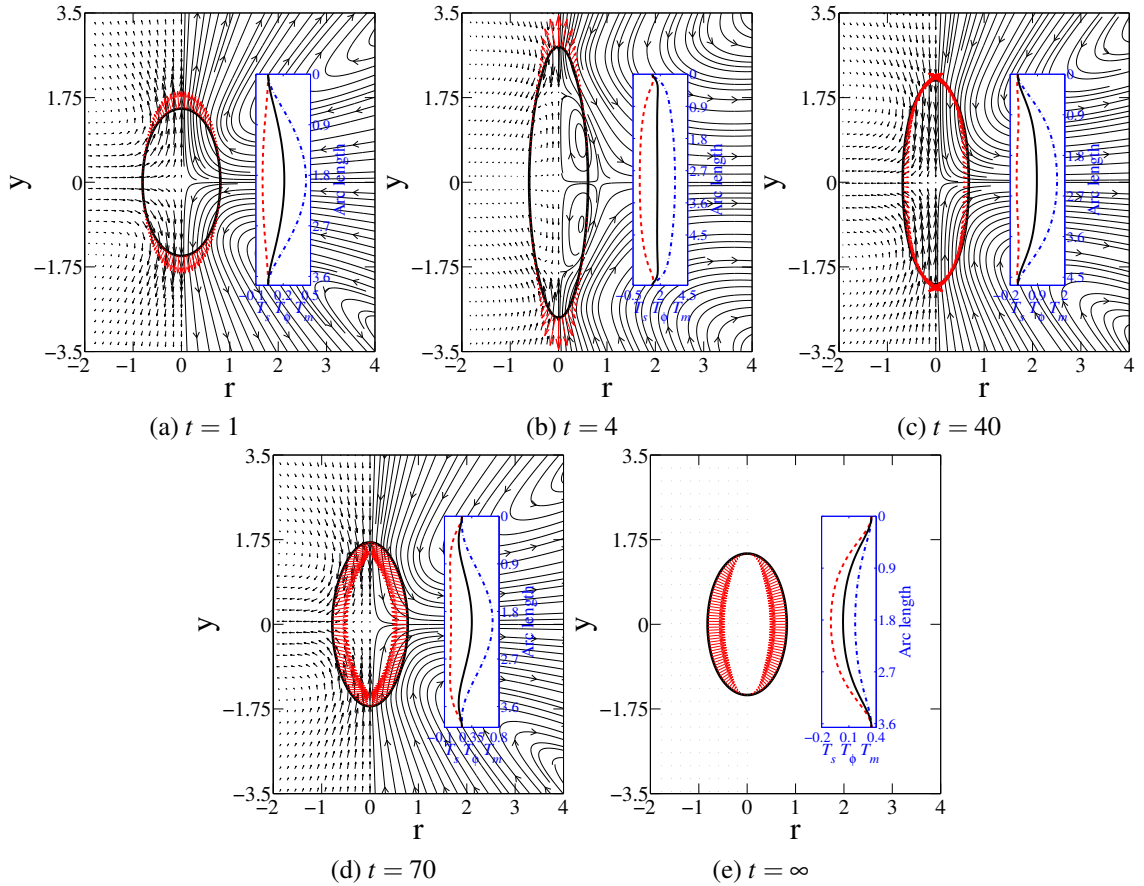


Figure 11: Stream line plot (curves with arrow, shown only at right side of axis of symmetry), velocity profile (short arrows, magnitude represents extend of flow, shown only at left side of axis of symmetry) and electric stress (arrows from the interface) for  $Ca = 2$  and  $\sigma_r = 10$  at different times. Inset shows the variation of meridional,  $T_s$  (— · —), azimuthal,  $T_\phi$  (— —) and mean,  $T_m$  (—) membrane tensions along the arc length.

#### 4.4 Effect of membrane capacitance, conductance and hydrodynamics on capsule deformation

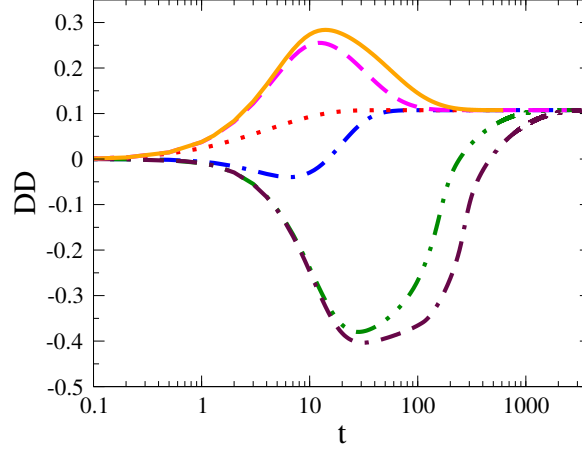


Figure 12: Effect of membrane capacitance on the dynamics of deformation of a capsule with Skalak membrane considering  $\hat{G}_m = 0$  at  $Ca = 0.25$ . Curves with line-style  $(\dots)$  for  $\hat{C}_m = 1$ ,  $(- -)$  for  $\hat{C}_m = 50$   $(-)$  for  $\hat{C}_m = 100$  at  $\sigma_r = 10$  and curves with line-style  $(- \cdot -)$  for  $\hat{C}_m = 1$ ,  $(- \cdot -)$  for  $\hat{C}_m = 50$  and  $(- - \cdot)$  for  $\hat{C}_m = 100$  at  $\sigma_r = 0.1$ .

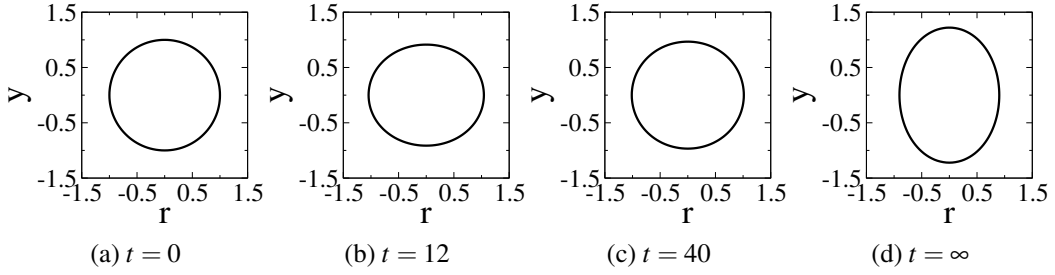


Figure 13: Shape evolution of a capsule with Skalak membrane at  $\hat{C}_m = 1$  for  $\sigma_r = 0.1$  and  $Ca = 0.45$ .

Figure 12 shows the effect of membrane capacitance on the degree of deformation of a capsule. As the capacitance increases the response becomes slower, since the charging time increases. For  $\sigma_r = 10$ , where prolate deformation is expected, the peak deformation for higher capacitances is higher because the continuity of Ohmic current in the fluid and the displacement current in the membrane, means that higher the capacitance higher is the normal electric field in the two fluids. This leads to higher Maxwell stress. A similar explanation can be provided for the oblate deformation observed when  $\sigma_r = 0.1$ . Moreover, as expected, the relaxation time is higher for higher capacitances. Lower capacitances, also mean faster charging of the membrane, higher membrane impedance at short times, which negate the drop-like behavior of a capsule at short times, since  $t_{cap} \sim t_{MW} \sim t_H$ . Very small oblate intermediate deformation are therefore observed at  $\sigma_r = 0.1$ , when  $\hat{C}_m = 1$ .

Figure 13 shows that the intermediate shapes obtained during the deformation of capsules with small capacitances are quite different compared to those for high capacitances. A capsule ( $Ca = 0.45$  and  $\sigma_r = 0.1$ ), deforms into an oblate spheroid (fig. 13b) shape and through an intermediate near spherical shape (fig. 13c) it reaches to a steady state prolate spheroid (fig. 13d). The absence of squaring is really due to absence of high compressive stresses, observed in the high capacitance

case, since the membrane already becomes charged enough, to negate the effect of build up of Maxwell stress due to conductivity contrast. The steady state prolate shape is independent of the membrane capacitance. This suggests that for admitting intermediate squaring and biconcave shapes a sufficiently high capacitance of the membrane is essential.

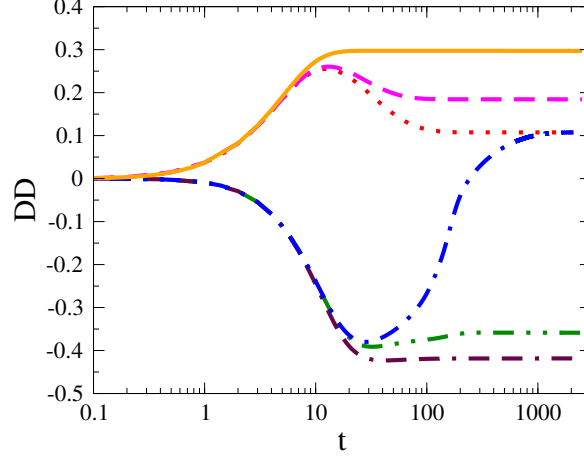


Figure 14: Effect of membrane conductance on the deformation of a capsule with Skalak membrane considering  $\hat{C}_m = 50$  at  $Ca = 0.25$ . Curves with line-style ( $\cdots$ ) for  $\hat{G}_m = 0$ , ( $---$ ) for  $\hat{G}_m = 1$  ( $---$ ) for  $\hat{G}_m = 10$  at  $\sigma_r = 10$  and curves with line-style ( $-\cdot-$ ) for  $\hat{G}_m = 0$ , ( $-\cdot\cdot-$ ) for  $\hat{G}_m = 1$  and ( $-\cdot-$ ) for  $\hat{G}_m = 10$  at  $\sigma_r = 0.1$ .

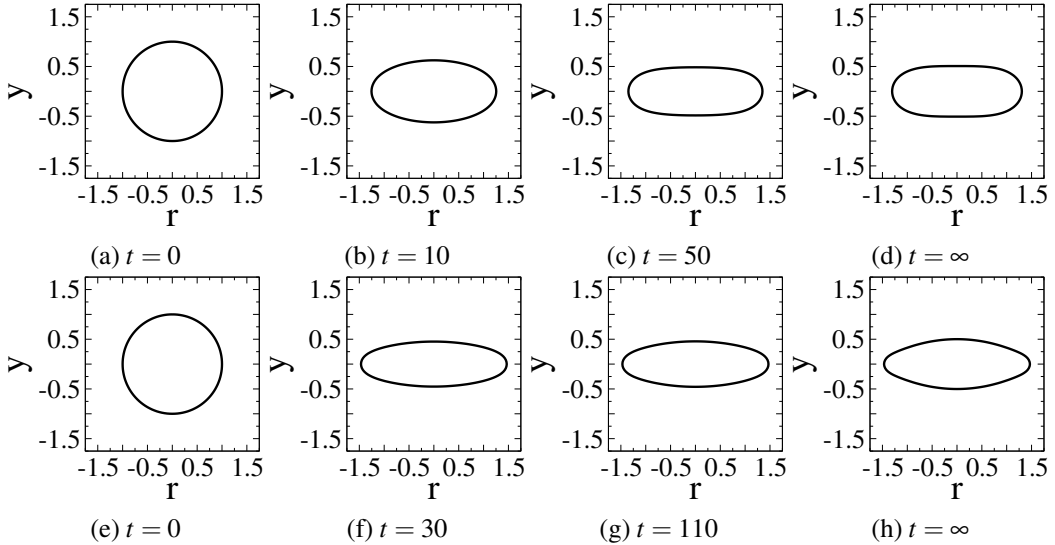


Figure 15: Shape evolution of a capsule with Skalak membrane at  $\sigma_r = 0.1$  for  $Ca = 0.45$  and  $\hat{C}_m = 50$  for conducting membrane. Figures a-d represent shapes during deformation at  $\hat{G}_m = 1$  and figs. e-h represent shapes during deformation at  $\hat{G}_m = 10$ .

The effect of membrane conductance on the degree of deformation is presented in fig. 14. For  $\sigma_r = 10$ , showing prolate deformation, the steady state deformation depends upon the membrane conductance. In the limit of the membrane conductance going to infinity, the steady state deformation is same as that of a liquid drop. Thus when  $\sigma_r = 0.1$ , the steady state deformation can be oblate, especially at high membrane conductances (note for  $\hat{G}_m = 0$ , the steady state deformation is always prolate), which correspond to oblate deformation observed even in liquid drops. This is

essentially due to a decrease in the membrane resistance and thereby the transmembrane potential going to zero.

For different values of membrane conductance, the dynamics (fig. 14) as well as the final steady state deformation and shapes are different (fig. 15). For both the small ( $\hat{G}_m = 1$  in figs. 15a to 15d) and large ( $\hat{G}_m = 10$  in figs. 15e to 15h) membrane conductance final steady state oblate shapes are observed ( $\sigma_r = 0.1$ ) unlike prolate steady state shapes for  $\hat{G}_m = 0$ .

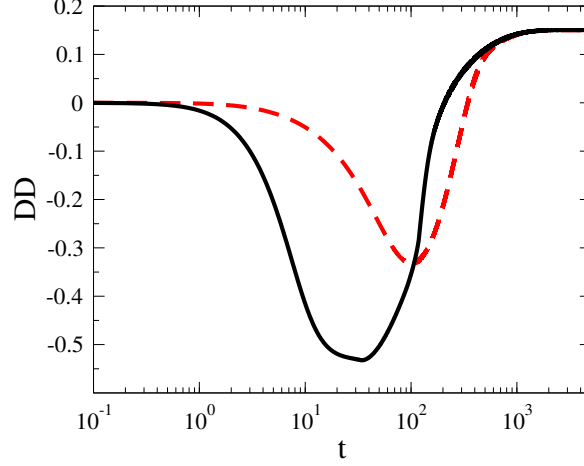


Figure 16: Comparison of the numerical simulation results for the dynamics of capsule deformation with  $t_H = 10$  (---) and  $t_H = 1$  (—) for  $Ca = 0.45$  and  $\sigma_r = 0.1$ .

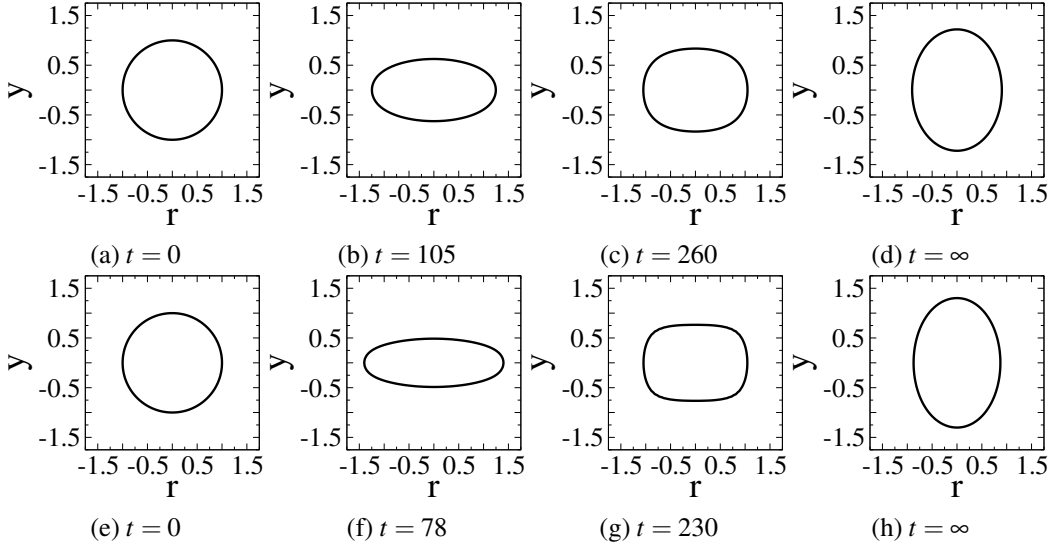


Figure 17: Shape evolution of a capsule with Skalak membrane at  $\sigma_r = 0.1$ ,  $\varepsilon_r = 1$  with  $t_H = 10$  for nonconducting membrane with  $\hat{C}_m = 50$ . Figures a-d represent shapes during deformation at  $Ca = 0.45$  and figures e-h represent deformed shapes at  $Ca = 0.8$ .

When the hydrodynamic response time ( $t_H$ ) is greater than 1 (in this case  $t_H = 10$ ,  $Ca = 0.45$  and  $\sigma_r = 0.1$  are considered), a capsule undergoes much smaller intermediate deformation. Figure 16 shows that although the membrane electrostatic stresses are high at  $t \sim t_e$ , a sphere does not deform due to slow hydrodynamic relaxation. By the time the capsule shape responds to the stresses, the electric stresses themselves have already relaxed over time scales of  $t \sim t_{cap}$ . Thus  $t_H$  plays a critical

role in the formation of biconcave intermediate shapes as well as squaring and hexagonal shapes discussed earlier. This is essentially due to the  $t_H = t_e$  parameters chosen in those calculations. In that case, the shape responds instantaneously to the applied electric stress. Figures 17a to 17d, show that a capsule does not attain intermediate biconcave and hexagonal shapes. Moreover, the squaring also become less prominent. At  $Ca = 0.8$  too, biconcave and hexagonal intermediate shapes are not admitted, although squaring of the capsule is observed (figs. 17e to 17h). Further increase in capillary number results in failure of the boundary integral code on account of numerical stiffness at the corners of the square shapes due to high curvature.

#### 4.5 Deformation as a function of capillary number and capsule break up

It is interesting to understand the role of constitutive equations and resulting membrane stresses in deformation of a capsule. For  $\sigma_r = 0.1$ , capsules with neo-Hookean membrane undergo a larger intermediate deformation compared to a capsule with Skalak membrane (fig. 18), even though the final steady state deformations are same at a particular capillary number (inset of fig. 18). Capsules undergo breakup at the intermediate maximum deformation at  $Ca = 0.46$  for Skalak membrane (fig. 19a) and at  $Ca = 0.3$  for neo-Hookean membrane (fig. 19c), therefore the calculations cannot be continued further.

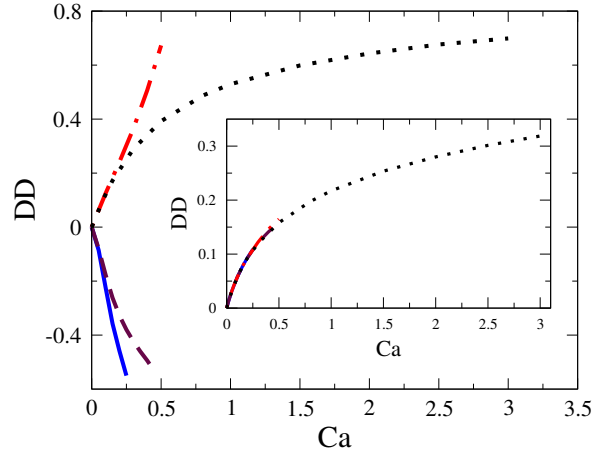


Figure 18: Intermediate maximum degree of deformation as a function of capillary number represented by curves (— · —) and (—) for neo-Hookean membrane at  $\sigma_r = 10$  and  $0.1$ , respectively where as curves ( $\cdots$ ) and (— —) for Skalak membrane at  $\sigma_r = 10$  and  $0.1$ , respectively. Inset shows the degree of deformation at steady state as a function of capillary number for the corresponding cases.

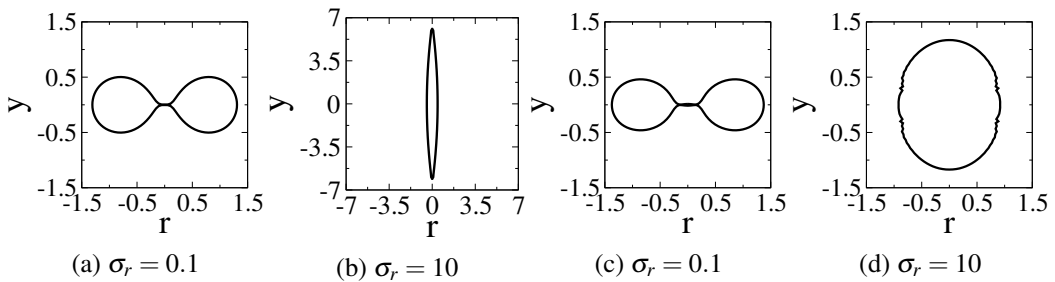


Figure 19: Break up shapes for a capsule with Skalak membrane at (a)  $Ca = 0.46$  and (b)  $Ca = 30$  and neo-Hookean membrane at (c)  $Ca = 0.3$  and (d)  $Ca = 0.5$ .



For  $\sigma_r = 10$ , at large capillary numbers, a neo-Hookean capsule shows strain softening behavior and undergoes very large maximum deformation, whereas a capsule with Skalak membrane shows strain hardening behavior in the maximum deformation as well as in the steady state deformation (fig. 18). Interestingly, both neo-Hookean membrane as well as Skalak membranes undergo possible breakup (which is manifested as a numerical singularity in our calculations) for  $\sigma_r = 0.1$ . A capsule with strain hardening Skalak membrane does not show breakup for fairly high value of capillary number (numerical failure takes place at  $Ca \sim 30$ ) for  $\sigma_r = 10$  (fig. 19b), whereas a capsule with neo-Hookean membrane shows a numerical singularity which is most likely a numerical artifact, at fairly low values of capillary number ( $Ca = 0.5$  as shown in fig. 19d).

## 5 Conclusions

Our analysis of an elastic capsule under electric field indicates that several timescales are involved,  $t_e$ ,  $t_{cap}$ ,  $t_{MW}$  and  $t_H$  in the deformation of an elastic capsule undergoing deformation in an applied uniform electric field. The fluids undergo transition from perfect dielectrics to leaky dielectrics, over  $t \sim t_{MW}$ , the capsule relaxes over time scales  $t_H$ , whereas the capacitor is charged over time scales  $t_{cap}$ , wherein it builds a transmembrane potential  $\phi_m = 3/2$ . An interplay of these time scales leads to a rich behavior in the response of elastic capsules to DC fields. Experiments on capsules in DC fields can thus enable estimation of electro-mechanical properties of these capsules.

Moreover, experimental analysis of a capsule in millisecond to microsecond pulsed electric fields should be able to show all the intermediate shape transitions, since the typical time required for the shape transition, reported in this work, is of the order of non-dimensional time  $t = 200$  and the considered timescale  $t_e$  varies in the range of  $[10^{-5}s - 10^{-7}s]$ , depending upon the nature of the external fluid.

The predictions of highly nonlinear shapes such as squaring of capsules, akin to those seen in vesicles (in experiments and simulations) confirms the appropriateness of this model to predict deformation of capsules in high fields, such as in electroporation, which has technological relevance. This study also paves the way to understand simultaneous deformation and breakup of more complex biological elastic capsules such as blood cells, and will be a topic of a future study.

## Acknowledgment

Authors would like to acknowledge Department of Science and Technology, India for financial support for this work.

## References

- D. Barthès-Biesel and J. M. Rallison. The time-dependent deformation of a capsule freely suspended in a linear shear flow. *Journal of Fluid Mechanics*, 113:251–267, 12 1981.
- R. B. Karyappa, S. D. Deshmukh, and R. M. Thaokar. Deformation of an elastic capsule in a uniform electric field. *Physics of Fluids*, 26(12):122108, 2014a. doi: 10.1063/1.4903838.

- K. Kataoka, A. Harada, and Y. Nagasaki. Block copolymer micelles for drug delivery: design, characterization and biological significance. *Advanced Drug Delivery Reviews*, 47(1):113 – 131, 2001. ISSN 0169-409X. Nanoparticulate Systems for Improved Drug Delivery.
- M. J. Lighthill. Pressure-forcing of tightly fitting pellets along fluid-filled elastic tubes. *Journal of Fluid Mechanics*, 34(1):113–143, 10 1968.
- W. A. Hyman and R. Skalak. Non-newtonian behavior of a suspension of liquid drops in tube flow. *AIChE Journal*, 18(1):149–154, 1972. ISSN 1547-5905.
- A. E. Green and J. E. Adkins. *large elastic deformation*. The Oxford University Press, London, 2 edition, 1970.
- R. Skalak, A. Tozeren, R.P. Zarda, and S. Chien. Strain energy function of red blood cell membranes. *Biophysical Journal*, 13(3):245 – 264, 1973. ISSN 0006-3495.
- C. Gao, S. Leporatti, S. Moya, E. Donath, and H. Möhwald. Stability and mechanical properties of polyelectrolyte capsules obtained by stepwise assembly of poly(styrenesulfonate sodium salt) and poly(diallyldimethyl ammonium) chloride onto melamine resin particles. *Langmuir*, 17(11): 3491–3495, 2001.
- A. Fery and R. Weinkamer. Mechanical properties of micro- and nanocapsules: Single-capsule measurements. *Polymer*, 48(25):7221 – 7235, 2007. ISSN 0032-3861.
- M. W. Keller and N. R. Sottos. Mechanical properties of microcapsules used in a self-healing polymer. *Experimental Mechanics*, 46(6):725–733, 2006. ISSN 1741-2765.
- F. Dubreuil, N. Elsnér, and A. Fery. Elastic properties of polyelectrolyte capsules studied by atomic-force microscopy and ricm. *The European Physical Journal E*, 12(2):215–221, 2003. ISSN 1292-895X.
- K. S. Chang and W. L. Olbricht. Experimental studies of the deformation of a synthetic capsule in extensional flow. *Journal of Fluid Mechanics*, 250:587–608, 005 1993.
- D. Barthès-Biesel. Motion of a spherical microcapsule freely suspended in a linear shear flow. *Journal of Fluid Mechanics*, 100(4):831–853, 10 1980.
- D. Barthès-Biesel and V. Chhim. The constitutive equation of a dilute suspension of spherical microcapsules. *International Journal of Multiphase Flow*, 7(5):493 – 505, 1981. ISSN 0301-9322.
- D. Barthès-Biesel. Role of interfacial properties on the motion and deformation of capsules in shear flow. *Physica A: Statistical Mechanics and its Applications*, 172(1):103 – 124, 1991. ISSN 0378-4371.
- J.-W. Ha and S.-M. Yang. Electrohydrodynamic effects on the deformation and orientation of a liquid capsule in a linear flow. *Physics of Fluids*, 12(7):1671–1684, 2000.
- R. M. Thaokar. Time-dependent electrohydrodynamics of a compressible viscoelastic capsule in the small-deformation limit. *Phys. Rev. E*, 94:042607, Oct 2016.
- S. Kessler, R. Finken, and U. Seifert. Elastic capsules in shear flow: Analytical solutions for constant and time-dependent shear rates. *The European Physical Journal E*, 29(4):399–413, Aug 2009. ISSN 1292-895X.
- R. Finken, S. Kessler, and U. Seifert. Micro-capsules in shear flow. *Journal of Physics: Condensed Matter*, 23(18):184113, 2011.
- H. Zhou and C. Pozrikidis. Deformation of liquid capsules with incompressible interfaces in

- simple shear flow. *Journal of Fluid Mechanics*, 283:175–200, 001 1995. doi: 10.1017/S0022112095002278.
- P. R. Rao, G. I. Zahalak, and S. P. Sutera. Large deformations of elastic cylindrical capsules in shear flows. *Journal of Fluid Mechanics*, 270:73–90, 007 1994.
- C. Pozrikidis. Finite deformation of liquid capsules enclosed by elastic membranes in simple shear flow. *Journal of Fluid Mechanics*, 297:123–152, 008 1995.
- S. Ramanujan and C. Pozrikidis. Deformation of liquid capsules enclosed by elastic membranes in simple shear flow: large deformations and the effect of fluid viscosities. *Journal of Fluid Mechanics*, 361:117–143, 04 1998.
- C. Pozrikidis. Effect of membrane bending stiffness on the deformation of capsules in simple shear flow. *Journal of Fluid Mechanics*, 440:269–291, 08 2001.
- D. V. Le. Effect of bending stiffness on the deformation of liquid capsules enclosed by thin shells in shear flow. *Phys. Rev. E*, 82:016318, Jul 2010.
- S. Kessler, R. Finken, and U. Seifert. Swinging and tumbling of elastic capsules in shear flow. *Journal of Fluid Mechanics*, 605:207–226, 006 2008. doi: 10.1017/S0022112008001493.
- Y. Sui, H. T. Low, Y. T. Chew, and P. Roy. Tank-treading, swinging, and tumbling of liquid-filled elastic capsules in shear flow. *Phys. Rev. E*, 77:016310, Jan 2008a.
- Y. Sui, Y. T. Chew, P. Roy, and H. T. Low. Effect of membrane bending stiffness on the deformation of elastic capsules in extensional flow: A lattice boltzmann study. *International Journal of Modern Physics C*, 18(08):1277–1291, 2007.
- Y. Sui, X.B. Chen, Y.T. Chew, P. Roy, and H.T. Low. Numerical simulation of capsule deformation in simple shear flow. *Computers & Fluids*, 39(2):242 – 250, 2010. ISSN 0045-7930.
- J. M. Skotheim and T. W. Secomb. Red blood cells and other nonspherical capsules in shear flow: Oscillatory dynamics and the tank-treading-to-tumbling transition. *Phys. Rev. Lett.*, 98:078301, Feb 2007.
- Y. Navot. Elastic membranes in viscous shear flow. *Physics of Fluids*, 10(8):1819–1833, 1998. doi: 10.1063/1.869702.
- E. Lac, D. Barthès-Biesel, N. A. Pelekasis, and J. Tsamopoulos. Spherical capsules in three-dimensional unbounded stokes flows: effect of the membrane constitutive law and onset of buckling. *Journal of Fluid Mechanics*, 516:303–334, 10 2004.
- E. Lac and D. Barthès-Biesel. Deformation of a capsule in simple shear flow: Effect of membrane prestress. *Physics of Fluids*, 17(7):072105, 2005. doi: 10.1063/1.1955127.
- Y. Sui, Y.T. Chew, P. Roy, and H.T. Low. A hybrid method to study flow-induced deformation of three-dimensional capsules. *Journal of Computational Physics*, 227(12):6351 – 6371, 2008b. ISSN 0021-9991.
- R. Finken and U. Seifert. Wrinkling of microcapsules in shear flow. *Journal of Physics: Condensed Matter*, 18(15):L185–L191, 2006.
- W. R. Dodson and P. Dimitrakopoulos. Dynamics of strain-hardening and strain-softening capsules in strong planar extensional flows via an interfacial spectral boundary element algorithm for elastic membranes. *Journal of Fluid Mechanics*, 641:263–296, 2009. doi: 10.1017/S0022112009991662.
- S. Kwak and C. Pozrikidis. Effect of membrane bending stiffness on the axisymmetric deformation

- of capsules in uniaxial extensional flow. *Physics of Fluids*, 13(5):1234–1242, 2001. doi: 10.1063/1.1352629.
- C. Dupont, A.-V. Salsac, D. Barthès-Biesel, M. Vidrascu, and P. L. Tallec. Influence of bending resistance on the dynamics of a spherical capsule in shear flow. *Physics of Fluids*, 27(5):051902, 2015.
- J. M. Crowley. Electrical breakdown of bimolecular lipid membranes as an electromechanical instability. *Biophysical Journal*, 13(7):711 – 724, 1973. ISSN 0006-3495.
- D. P. Tieleman. The molecular basis of electroporation. *BMC Biochemistry*, 5(1):10, Jul 2004. ISSN 1471-2091.
- E. Neumann, A.E. Sowers, and C.A. Jordan. *Electroporation and Electrofusion in Cell Biology*. Plenum press, New York, 1 edition, 1989.
- R. Pethig. Dielectrophoresis: Using inhomogeneous ac electrical fields to separate and manipulate cells. *Critical Reviews in Biotechnology*, 16(4):331–348, 1996.
- Y. Kang, D. Li, S. A. Kalams, and J. E. Eid. Dc-dielectrophoretic separation of biological cells by size. *Biomedical Microdevices*, 10(2):243–249, Apr 2008. ISSN 1572-8781.
- T. Yamamoto, S. Aranda-Espinoza, R. Dimova, and R. Lipowsky. Stability of spherical vesicles in electric fields. *Langmuir*, 26(14):12390–12407, 2010.
- R. M. Thaokar and S. D. Deshmukh. Rayleigh instability of charged drops and vesicles in the presence of counterions. *Physics of Fluids*, 22(3):034107, 2010.
- S. D. Deshmukh and R. M. Thaokar. Deformation, breakup and motion of a perfect dielectric drop in a quadrupole electric field. *Physics of Fluids*, 24(3):032105, 2012a.
- S. D. Deshmukh and R. M. Thaokar. Deformation and breakup of a leaky dielectric drop in a quadrupole electric field. *Journal of Fluid Mechanics*, 731:713–733, 2013a.
- R. B. Karyappa, S. D. Deshmukh, and R. M. Thaokar. Breakup of a conducting drop in a uniform electric field. *Journal of Fluid Mechanics*, 754:550–589, 2014b.
- S. Das, Y. S. Mayya, and R. Thaokar. Dynamics of a charged drop in a quadrupole electric field. *EPL (Europhysics Letters)*, 111(2):24006, 2015.
- L. C. McConnell, P. M. Vlahovska, and M. J. Miksis. Vesicle dynamics in uniform electric fields: squaring and breathing. *Soft Matter*, 11:4840–4846, 2015a. doi: 10.1039/C5SM00585J.
- M. Ouriemi and P. M. Vlahovska. Electrohydrodynamic deformation and rotation of a particle-coated drop. *Langmuir*, 31(23):6298–6305, 2015. doi: 10.1021/acs.langmuir.5b00774. PMID: 26011225.
- K. A. Riske and R. Dimova. Electric pulses induce cylindrical deformations on giant vesicles in salt solutions. *Biophysical Journal*, 91(5):1778 – 1786, 2006. ISSN 0006-3495.
- R. Dimova, K. A. Riske, S. Aranda, N. Bezlyepkina, R. L. Knorr, and R. Lipowsky. Giant vesicles in electric fields. *Soft Matter*, 3:817–827, 2007.
- R. Dimova, N. Bezlyepkina, M. D. Jordo, R. L. Knorr, K. A. Riske, M. Staykova, P. M. Vlahovska, T. Yamamoto, P. Yang, and R. Lipowsky. Vesicles in electric fields: Some novel aspects of membrane behavior. *Soft Matter*, 5:3201–3212, 2009.
- L. C. McConnell, M. J. Miksis, and P. M. Vlahovska. Continuum modeling of the electric-field-induced tension in deforming lipid vesicles. *The Journal of Chemical Physics*, 143(24):243132, 2015b.

- L. C. McConnell, M. J. Miksis, and P. M. Vlahovska. Vesicle electrohydrodynamics in dc electric fields. *IMA Journal of Applied Mathematics*, 78(4):797, 2013.
- S. Veerapaneni. Integral equation methods for vesicle electrohydrodynamics in three dimensions. *Journal of Computational Physics*, 326:278 – 289, 2016. ISSN 0021-9991.
- E. M. Kolahdouz and D. Salac. Electrohydrodynamics of three-dimensional vesicles: A numerical approach. *SIAM Journal on Scientific Computing*, 37(3):B473–B494, 2015a. doi: 10.1137/140988966.
- E. M. Kolahdouz and D. Salac. Dynamics of three-dimensional vesicles in dc electric fields. *Phys. Rev. E*, 92:012302, Jul 2015b.
- C. Grosse and H. P. Schwan. Cellular membrane potentials induced by alternating fields. *Biophysical Journal*, 63(6):1632 – 1642, 1992. ISSN 0006-3495.
- K. A. DeBruin and W. Krassowska. Modeling electroporation in a single cell. i. effects of field strength and rest potential. *Biophysical Journal*, 77(3):1213 – 1224, 1999. ISSN 0006-3495.
- D. Barthès-Biesel, A. Diaz, and E. Dhenin. Effect of constitutive laws for two-dimensional membranes on flow-induced capsule deformation. *Journal of Fluid Mechanics*, 460:211–222, 2002.
- W. F. Hu, Y. Kim, and M.-C. Lai. An immersed boundary method for simulating the dynamics of three-dimensional axisymmetric vesicles in navier-stokes flows. *Journal of Computational Physics*, 257, Part A:670 – 686, 2014. ISSN 0021-9991.
- J. M. Rallison and A. Acrivos. A numerical study of the deformation and burst of a viscous drop in an extensional flow. *Journal of Fluid Mechanics*, 89:191–200, 11 1978. ISSN 1469-7645.
- S. D. Deshmukh and R. M. Thaokar. Deformation, breakup and motion of a perfect dielectric drop in a quadrupole electric field. *Physics of Fluids*, 24(3):032105, 2012b.
- S. D. Deshmukh and R. M. Thaokar. Deformation and breakup of a leaky dielectric drop in a quadrupole electric field. *Journal of Fluid Mechanics*, 731:713–733, 9 2013b.
- C. Pozrikidis. The axisymmetric deformation of a red blood cell in uniaxial straining stokes flow. *Journal of Fluid Mechanics*, 216:231–254, 1990. ISSN 1469-7645.
- J. T. Schwalbe, P. M. Vlahovska, and M. J. Miksis. Vesicle electrohydrodynamics. *Phys. Rev. E*, 83: 046309, Apr 2011.

## Appendices

### A Analytical solution

Electrostatics and hydrodynamics of capsule deformation are solved analytically in spherical coordinate system  $(r, \theta, \phi)$ , where  $r$ ,  $\theta$  and  $\phi$  are the measurements of radial distance, meridional and azimuthal angles.

## A.1 Solution for the electrostatics

### A.1.1 Analytical electrostatic theory (AET)

The external and internal potentials because of the external uniform electric field of intensity  $E_0$  of a spherical interface can be represented using spherical harmonics.

$$\phi_i = A_1 r \cos(\theta) \quad (21)$$

$$\phi_e = B_1 \cos(\theta)/r^2 - r \cos(\theta), \quad (22)$$

where  $A_1$  and  $B_1$  are time dependent coefficients of spherical harmonics. The time dependent transmembrane potential is expressed as

$$\phi_m = \phi_{amp} \cos(\theta), \quad (23)$$

where  $\phi_{amp} = \phi_i - \phi_e$  is the amplitude of the transmembrane potential. Current continuity condition across the membrane is expressed by

$$\sigma_r E_{n,i} + \epsilon_r \frac{dE_{n,i}}{dt} = E_{n,e} + \frac{dE_{n,e}}{dt} = \hat{C}_m \frac{d\phi_m}{dt} + \hat{G}_m \phi_m \quad (24)$$

In these non-dimensional equations, one can recall that  $\hat{C}_m = C_m a / (\epsilon_e \epsilon_0)$  and  $\hat{G}_m = a G_m / \sigma_e$ . Solving section A.1.1 along with eq. (23) and eq. (24) coefficients  $A_1$  and  $B_1$  are obtained, and the analytical expressions are very large and cumbersome to evaluate. Internal and external normal electric fields are obtained as

$$\mathbf{E}_{n,i} = -\mathbf{n} \cdot \nabla \phi_i \quad (25)$$

$$\mathbf{E}_{n,e} = -\mathbf{n} \cdot \nabla \phi_e \quad (26)$$

and tangential fields as

$$\mathbf{E}_{t,i} = -\mathbf{t} \cdot \nabla \phi_i \quad (27)$$

$$\mathbf{E}_{t,e} = -\mathbf{t} \cdot \nabla \phi_e. \quad (28)$$

Normal and tangential electric stresses can be obtained from

$$\tau_n^E = \frac{1}{2} Ca [(\mathbf{E}_{n,e}^2 - \mathbf{E}_{t,e}^2) - \epsilon_r (\mathbf{E}_{n,i}^2 - \mathbf{E}_{t,i}^2)], \quad (29)$$

$$\tau_t^E = Ca [\mathbf{E}_{n,e} \mathbf{E}_{t,e} - \epsilon_r \mathbf{E}_{n,i} \mathbf{E}_{t,i}]. \quad (30)$$

Electric tractions acting on the interface are given by

$$f_x^E = \tau_n^E n_x + \tau_t^E t_x, \quad (31)$$

$$f_y^E = \tau_n^E n_y + \tau_t^E t_y. \quad (32)$$

Transmembrane potential at  $\hat{G}_m = 0$ ,  $\hat{C}_m = 50$ ,  $\epsilon_r = 1$  and  $\sigma_r = 1$  is obtained as

$$\phi_m = \frac{3}{2} (1 - e^{-t/76}) \cos \theta, \quad (33)$$

and normal and tangential stresses are obtained as

$$\tau_n = \frac{1}{8}Ca \left( 3e^{-t/38} \sin^2 \theta + 6e^{-t/76} \sin^2 \theta - 9 \sin^2 \theta \right) \quad (34)$$

$$\tau_t = -\frac{3}{4}Ca \left( e^{-t/76} - 1 \right) e^{-t/38} \sin(2\theta). \quad (35)$$

For  $\sigma_r = 0.1$  and 10 analytical solutions for normal and tangential electrical stresses are very complicated and obtained as large expressions. Figures comparing results for transmembrane potential, tangential electric stress and normal electric stress obtained from analytical theory and boundary integral simulation can be obtained in section A.2 (figs. 20a to 20c for  $\sigma_r = 1$ , figs. 21a to 21c for  $\sigma_r = 10$  and figs. 22a to 22c  $\sigma_r = 0.1$ ).

### A.1.2 Simplified electrostatic model (SEM)

It is often a good approximation to neglect the displacement current in the two fluids, since it is expected to be much smaller than the capacitive current of the membrane, ( $\epsilon_e/\sigma_e \ll 1$  and  $\epsilon_i/\sigma_i \ll 1$ ). In this case, the electrostatics equations reduce to,

$$\sigma_r E_{n,i} = E_{n,e} = \hat{C}_m \frac{d\phi_m}{dt} + \hat{G}_m \phi_m \quad (36)$$

and for a non conducting membrane the transmembrane potential is obtained as

$$\phi_m = \frac{3}{2}(1 - e^{-t/t_{cap}}), \quad (37)$$

known as Schwan equation [Grosse and Schwan \[1992\]](#) and normal and tangential stresses are obtained as

$$\tau_t = \frac{9}{4} \left[ \frac{(2 + \sigma_r^2) e^{\frac{-2t}{t_{cap}}} - \sigma_r (2 + \sigma_r) e^{\frac{-t}{t_{cap}}}}{(2 + \sigma_r)^2} \right] \sin 2\theta \quad (38)$$

$$\tau_n = \frac{9}{8} \frac{4(\sigma_r^2 - 1) e^{\frac{-2t}{t_{cap}}} + \left[ (5\sigma_r^2 - 8) e^{\frac{-2t}{t_{cap}}} + 2\sigma_r (2 + \sigma_r) e^{\frac{-t}{t_{cap}}} - (2 + \sigma_r)^2 \right] \sin^2 \theta}{(2 + \sigma_r)^2}. \quad (39)$$

Obtained form of the expressions for tangential and normal stresses are different but produce same result obtained with the reported expressions of stresses by [Schwalbe et al. \[2011\]](#). To analytically solve the Electrohydrodynamics of capsule, simplified electrostatic model is used to calculate interfacial electric stresses. Formulation of the elastic traction (considering liner elasticity model with Poisson's ratio  $\nu_s = 1$ ), hydrodynamics and the solution methodology for the deformation of an elastic capsule are followed as reported by [Thaokar \[2016\]](#). The general expression for the degree of deformation is very large and complex. For  $\hat{G}_m = 0$ ,  $\hat{C}_m = 50$ ,  $\epsilon_r = 1$  degrees of deformation of



different conductivity ratios are obtained as

$$DD_{\sigma_r=0.1} = Ca \left[ -0.000193 + 0.0882e^{\frac{1}{5}\sqrt{\frac{31}{7}}t} + 0.703e^{\frac{1}{70}(21+\sqrt{217})t} - 2.125e^{\frac{311+15\sqrt{217}}{1050}t} + 0.014e^{\frac{313+15\sqrt{217}}{1050}t} \right] e^{-\frac{1}{70}(21+\sqrt{217})t} \quad (40)$$

$$DD_{\sigma_r=1} = Ca \left[ -0.00504 + 0.319e^{\frac{1}{5}\sqrt{\frac{31}{7}}t} + 0.703e^{\frac{1}{70}(21+\sqrt{217})t} - 1.122e^{\frac{287+15\sqrt{217}}{1050}t} + 0.106e^{\frac{301+15\sqrt{217}}{1050}t} \right] e^{-\frac{1}{70}(21+\sqrt{217})t} \quad (41)$$

$$DD_{\sigma_r=10} = Ca \left[ -0.00344 - 3.775e^{\frac{1}{5}\sqrt{\frac{31}{7}}t} + e^{\frac{1}{210}(49+3\sqrt{217})t} (4.887 + 0.333e^{\frac{1}{30}t} + 0.703e^{\frac{1}{15}t}) \right] e^{-\frac{1}{70}(21+\sqrt{217})t}. \quad (42)$$

Analytical and boundary integral simulation results for degree of deformation as a function of time at small capillary number are compared (fig. 23a, fig. 23c and fig. 23b for  $\sigma_r = 1, 0.1$  and  $10$ , respectively) considering  $\varepsilon_r = 1$ ,  $\hat{C}_m = 50$  and  $\hat{G}_m = 0$  for the validation of the boundary integral code, a very good match is obtained between numerical and analytical values.

## A.2 Validation of boundary integral code solving electric field

Boundary integral code with capacitor model (BEM-CM) to solve the electrostatics is validated comparing results with the analytical electrostatic theory (AET) considering  $\hat{G}_m = 0$ ,  $\hat{C}_m = 50$  and  $\varepsilon_r = 1$ . The evolution of transmembrane potential, normal and tangential stresses are shown in figs. 20a to 20c, respectively for  $\sigma_r = 1$ , figs. 21a to 21c, respectively for  $\sigma_r = 10$  and figs. 22a to 22c, respectively for  $\sigma_r = 0.1$ .

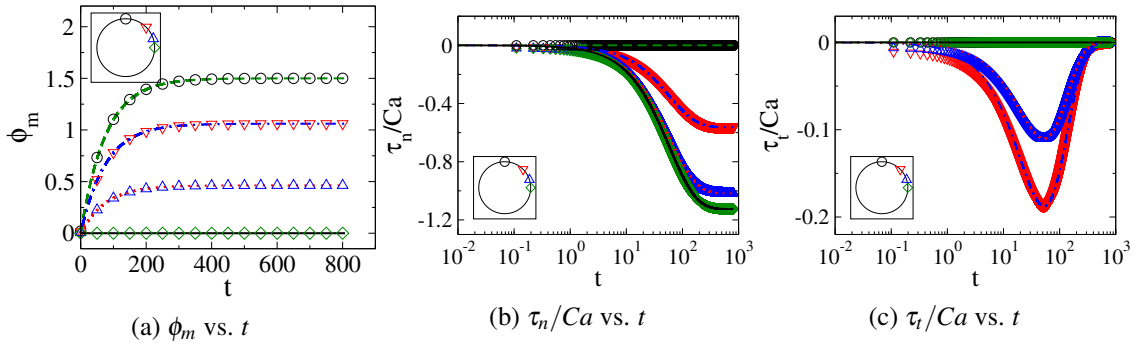


Figure 20: Comparison of numerically ( $\bigcirc$ ,  $\nabla$ ,  $\triangle$  and  $\diamond$  at  $\theta = 0, \pi/4, \pi/2.5$  and  $\pi/2$ , respectively) and analytically ( $—$ ,  $- - -$ ,  $\cdots$  and  $—$  at  $\theta = 0, \pi/4, \pi/2.5$  and  $\pi/2$ , respectively) obtained (a) transmembrane potential, (b) normal electric stress and (c) tangential electric stress as a function of time for  $\sigma_r = 1$ .

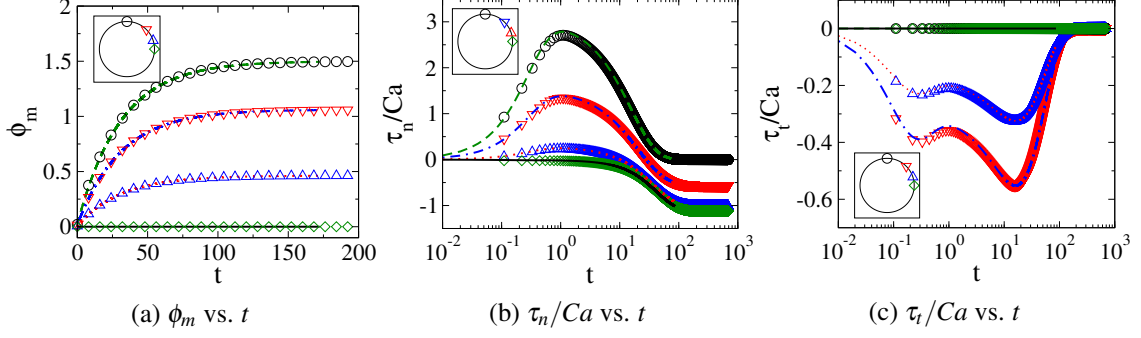


Figure 21: Comparison of numerically ( $\circ$ ,  $\nabla$ ,  $\triangle$  and  $\diamond$  at  $\theta = 0, \pi/4, \pi/2.5$  and  $\pi/2$ , respectively) and analytically ( $—$ ,  $- -$ ,  $\cdots$  and  $—$  at  $\theta = 0, \pi/4, \pi/2.5$  and  $\pi/2$ , respectively) obtained (a) transmembrane potential, (b) normal electric stress and (c) tangential electric stress as a function of time for  $\sigma_r = 10$ .

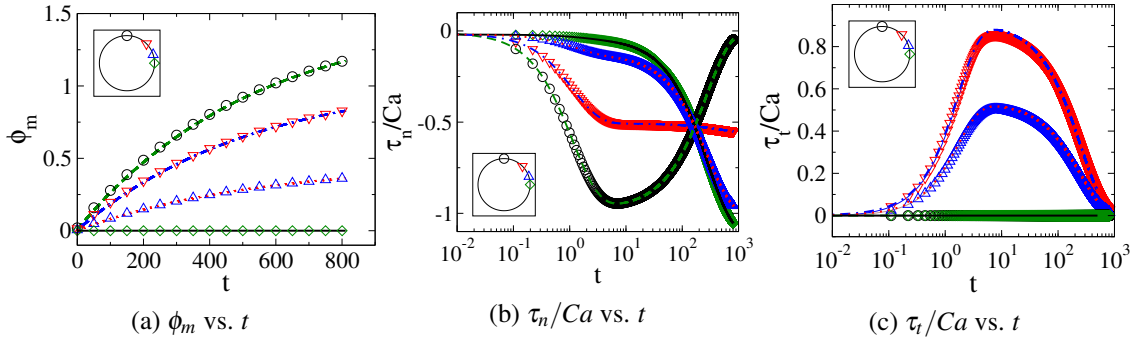


Figure 22: Comparison of numerically ( $\circ$ ,  $\nabla$ ,  $\triangle$  and  $\diamond$  at  $\theta = 0, \pi/4, \pi/2.5$  and  $\pi/2$ , respectively) and analytically ( $—$ ,  $- -$ ,  $\cdots$  and  $—$  at  $\theta = 0, \pi/4, \pi/2.5$  and  $\pi/2$ , respectively) obtained (a) transmembrane potential, (b) normal electric stress and (c) tangential electric stress as a function of time for  $\sigma_r = 0.1$ .

### A.3 Validation of boundary integral code for the deformation of capsule

Dynamics of deformation of a capsule with Skalak membrane obtained from analytical theory considering simplified electrostatic model (SEM), boundary integral method considering simplified capacitor model (BEM-SM) and boundary integral method considering capacitor model (BEM-CM) are compared at small capillary numbers ( $Ca = 0.01$  and  $Ca = 0.05$ ) for the validation of the BEM-CM which is used to study the dynamics of capsule deformation in this work. Considering  $\varepsilon_r = 1$ ,  $\hat{C}_m = 50$  and  $\hat{G}_m = 0$  dynamics are compared for  $\sigma_r = 1$ ,  $\sigma_r = 10$  and  $\sigma_r = 0.1$  in fig. 23a, fig. 23b and fig. 23c, respectively.

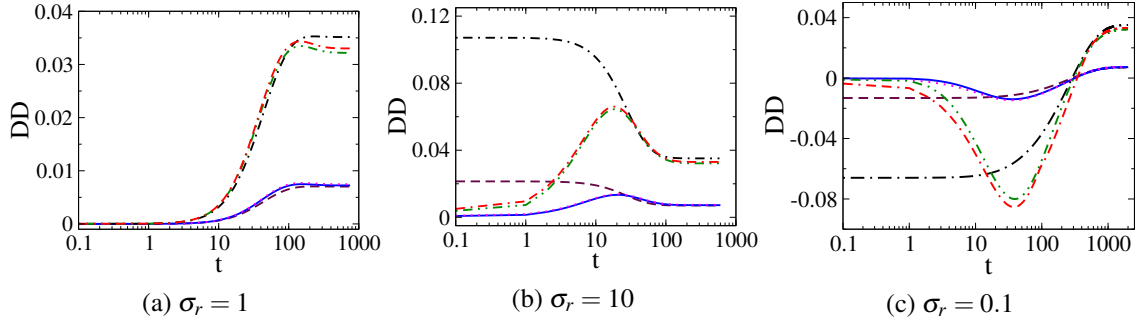


Figure 23: Comparison of dynamics obtained from SEM, BEM-SM and BEM-CM. At  $Ca = 0.01$  dynamics are represented by line-style (—) for SEM, ( $\cdots$ ) for BEM-SM and (—) for BEM-CM. At  $Ca = 0.05$  dynamics are represented by line-style ( $-\cdot-$ ) for SEM, ( $-\cdot-$ ) for BEM-SM and ( $-\cdot-$ ) for BEM-CM.

#### A.4 Importance of incorporating membrane bending

In the present study, the effect of bending rigidity is clearly demonstrated in fig. 24. Incorporating bending forces eliminate the formation of wiggles. However, it should be mentioned that for deformations with nominal curvatures, it was observed that the results of simulations with and without bending did not have significant differences.

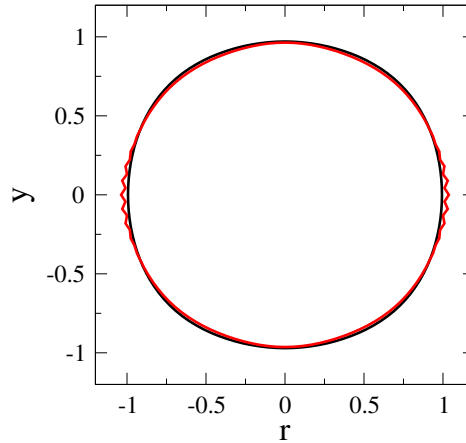


Figure 24: Effect of membrane bending rigidity on the deformation of a capsule with Skalak membrane considering  $\sigma_r = 0.1$  and  $Ca = 0.45$ . Continuous curve represents shape obtained from the boundary integral simulation without considering effect of bending rigidity and the dash-dotted curve represents the same with  $\kappa_b = 0.001$  at  $t = 196$ .

#### A.5 Dynamics of capsule with neo-Hookean membrane

Capsules with a neo-Hookean membrane show very similar intermediate shapes (figs. 25a to 25f) as observed for capsules with a Skalak membrane (figs. 6a to 6f) at  $Ca = 0.25$  and  $\sigma_r = 0.1$ . From the simulated shapes it can be observed that a neo-Hookean capsule passes through the squaring (figs. 25d and 25e) to a steady state prolate shape (fig. 25f).

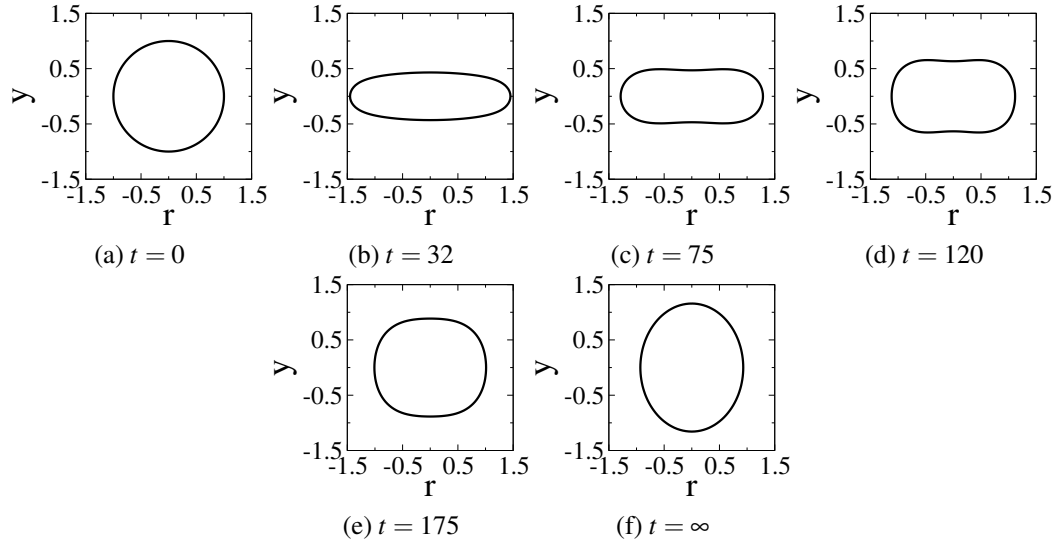


Figure 25: Shape evolution of a capsule with neo-Hookean membrane at  $\sigma_r = 0.1$  for  $Ca = 0.25$ .